The role of EMIC waves in the inner magnetosphere dynamics

Maria Usanova, LASP

email: Maria.Usanova@lasp.colorado.edu

Outline

#Observational platforms

#Magnetospheric plasma populations

#Wave-particle interactions

#EMIC waves

#Cold plasma heating

#Energetic particle precipitation

#Linkage to polar climate

#EMIC waves in planetary magnetospheres

Space monitoring: NASA Van Allen Probes mission

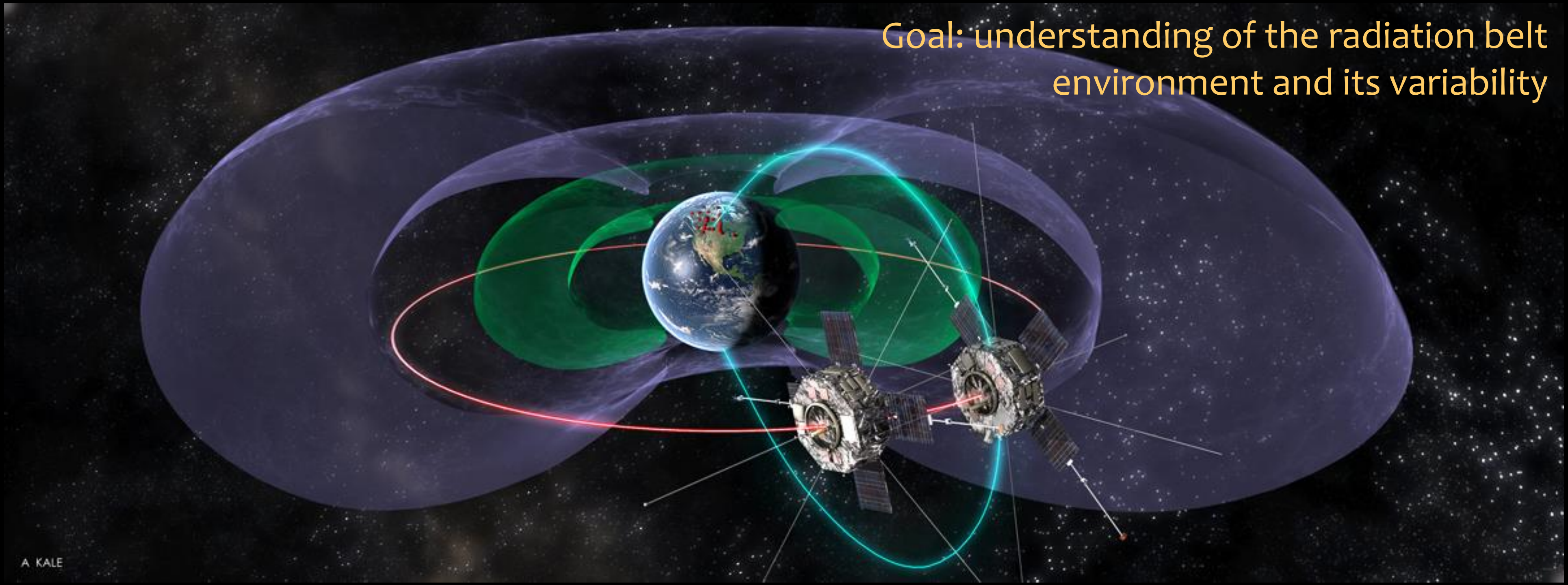

- Energetic Particle, Composition, and Thermal Plasma (ECT) Instrument Suite
- Electric and Magnetic Field Instrument Suite and Integrated Science (EMFISIS)
- Electric Field and Waves Instrument (EFW)
- Radiation Belt Storm Probes Ion Composition Experiment (RBSPICE)
- Relativistic Proton Spectrometer (RPS)

Space monitoring:
NASA Van Allen Probes mission

Launched on 30 Aug 2012
Image credit: Mike Killian

in conjunction
with cubesats at LEO,
stratospheric balloons
and ground magnetometers

Energetic electron precipitation

Bremsstrahlung X-rays

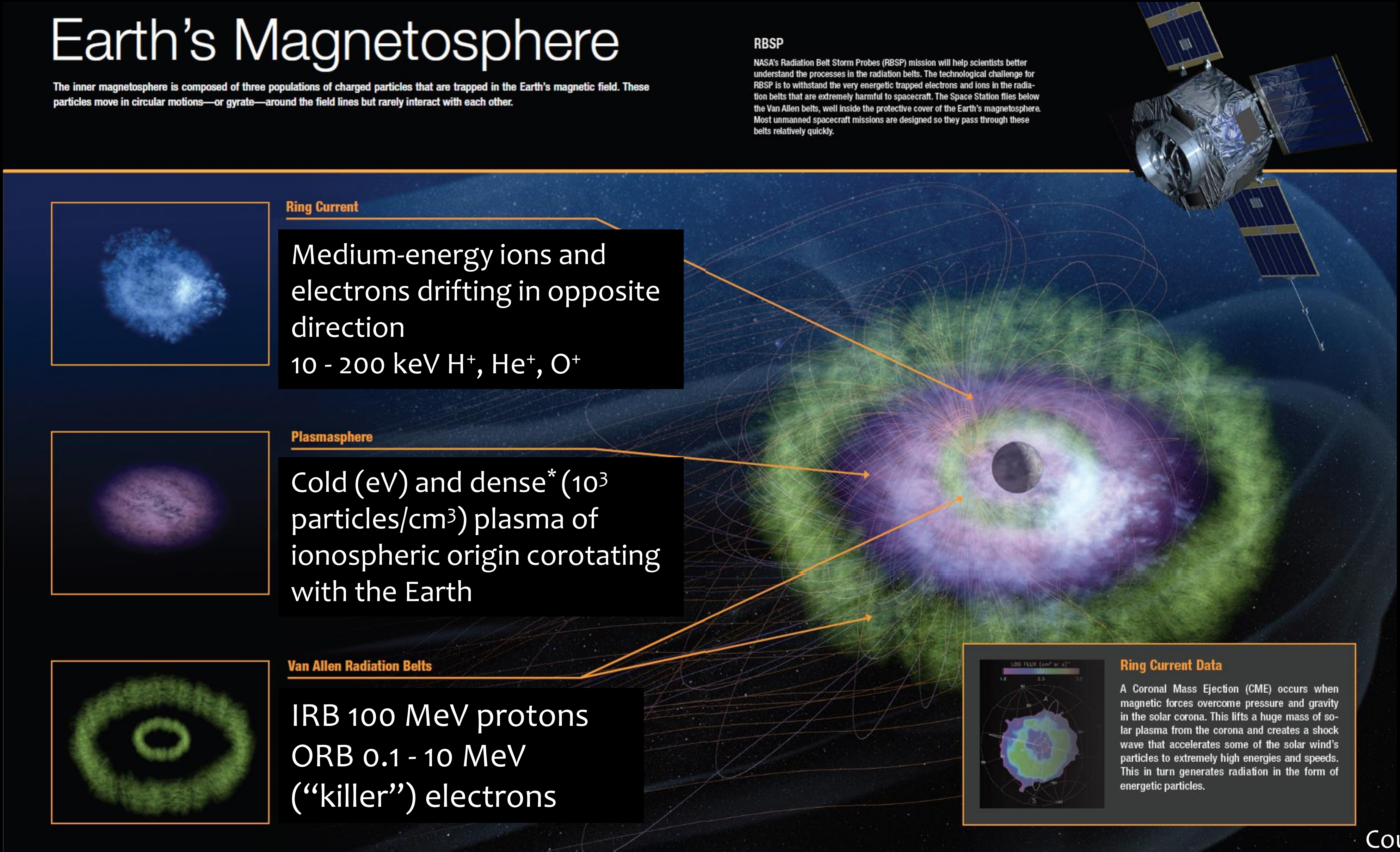

Medium-energy ions and electrons drifting in opposite direction
10 - 200 keV H^+, He^+, O^+

Cold (eV) and dense* (10^3 particles/cm^3) plasma of ionospheric origin corotating with the Earth

IRB 100 MeV protons
ORB 0.1 - 10 MeV ("killer") electrons

Courtesy: NASA

Reality is more complex…

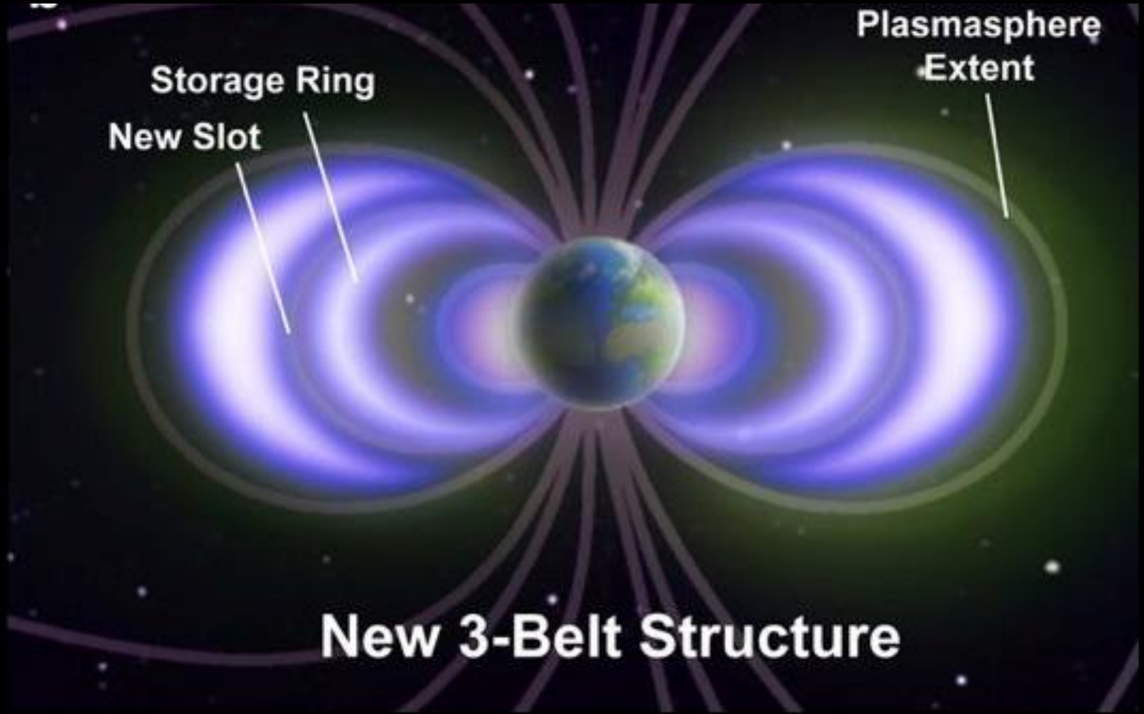

Van Allen Probes observed a three-belt structure at a few-MeV energies

Baker et a., Nature, 2012

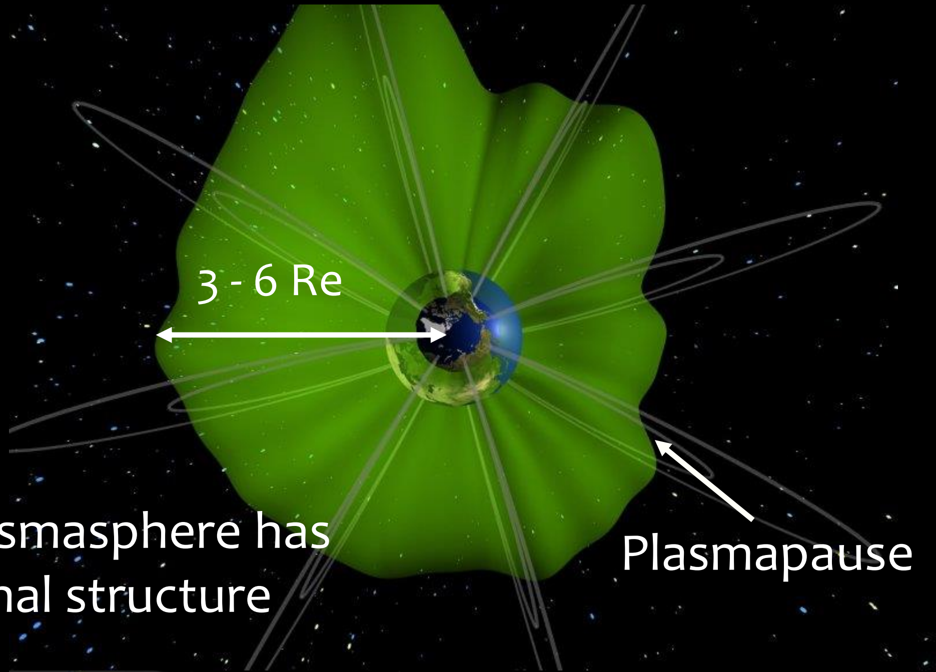

The plasmasphere has azimuthal structure

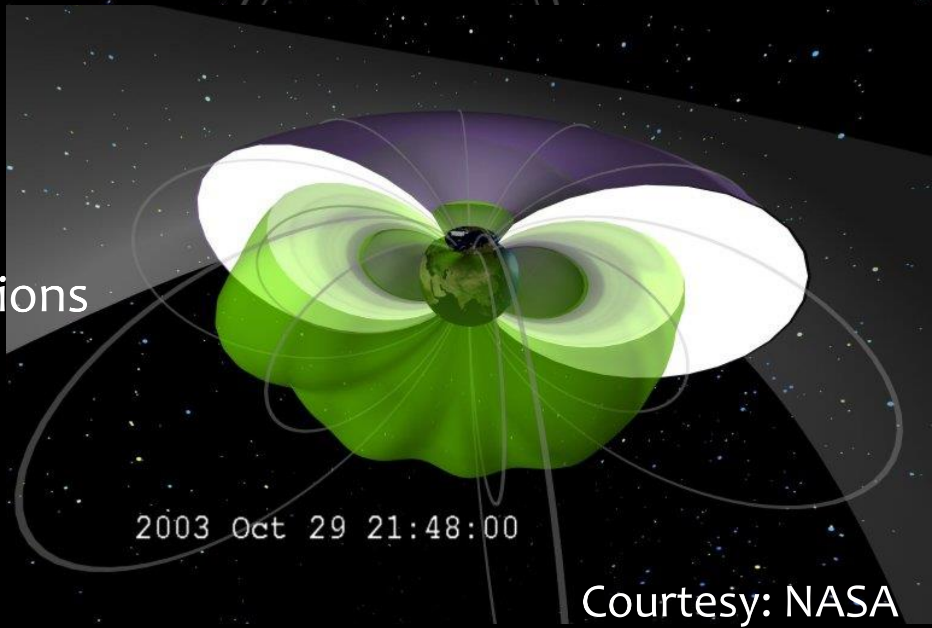

Different regions overlap

Courtesy: NASA

Balance between sources and losses

Sources

- Injections from the tail
- Wave-particle interactions
    - local acceleration
    - radial diffusion

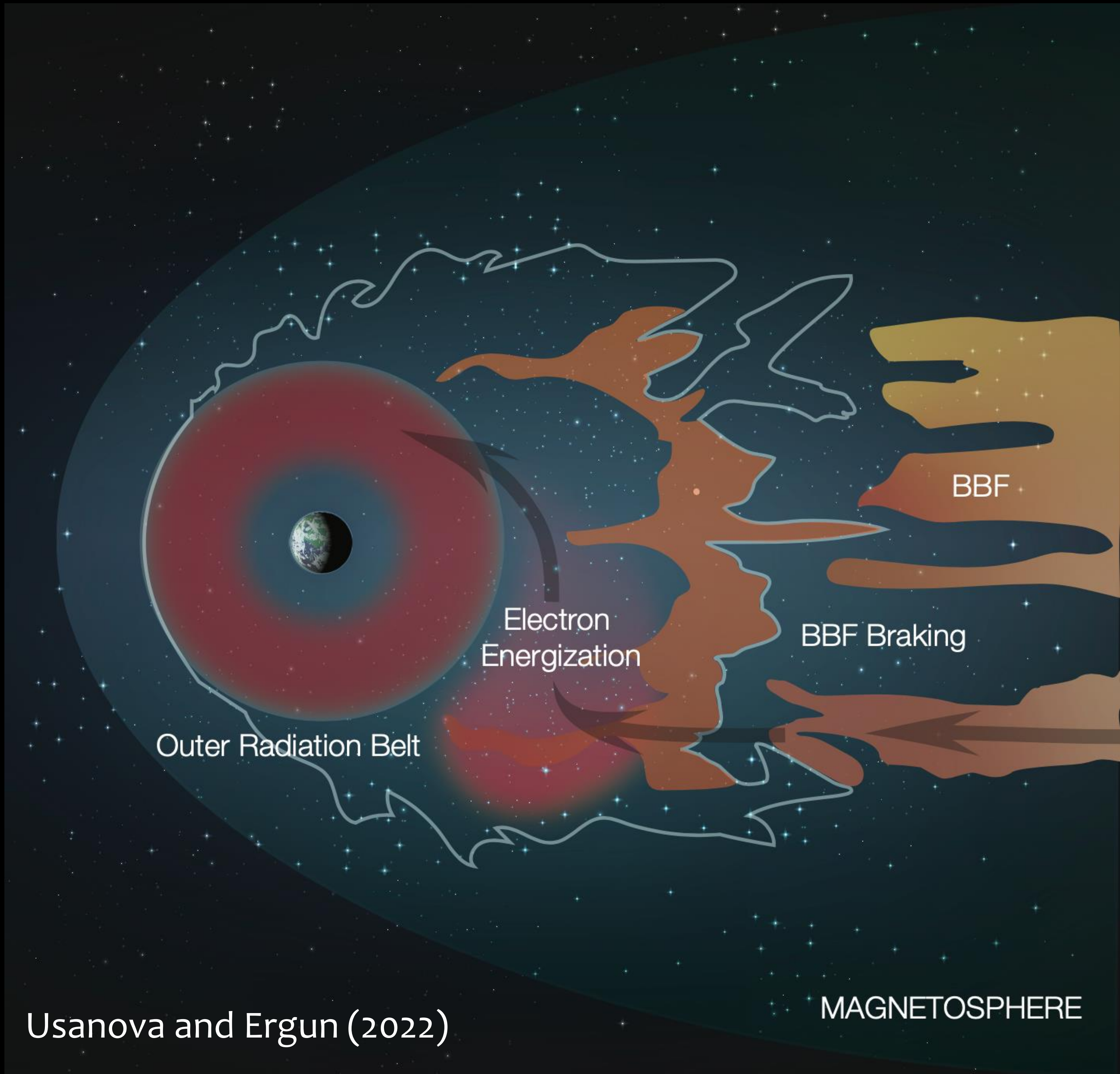

Usanova and Ergun (2022)

Losses

External: Magnetopause losses

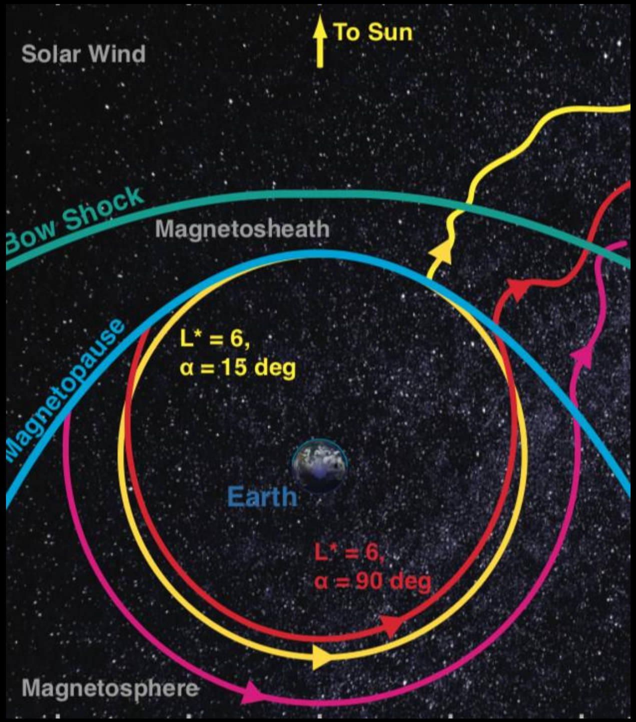

Turner and Ukhorskiy, 2020

1. Magnetopause shadowing

2. Outward radial diffusion

Internal: Losses to the atmosphere

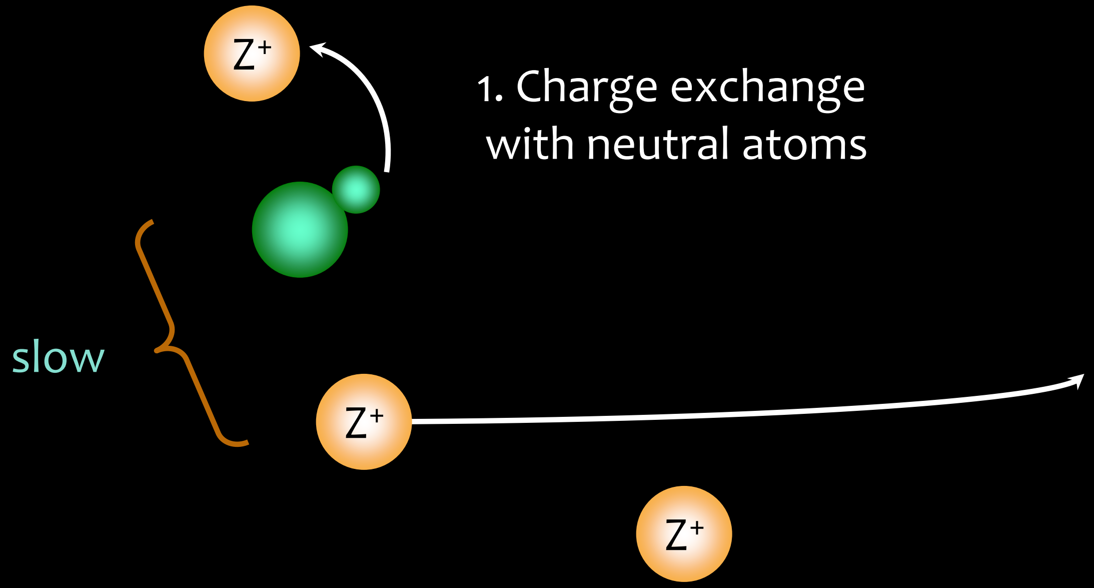

1. Charge exchange with neutral atoms

2. Coulomb collisions

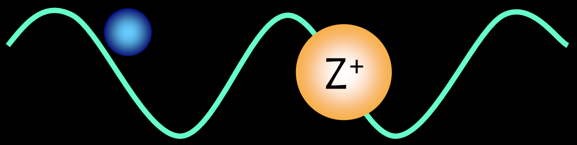

3. Wave-particle interactions

Why wave-particle interactions?

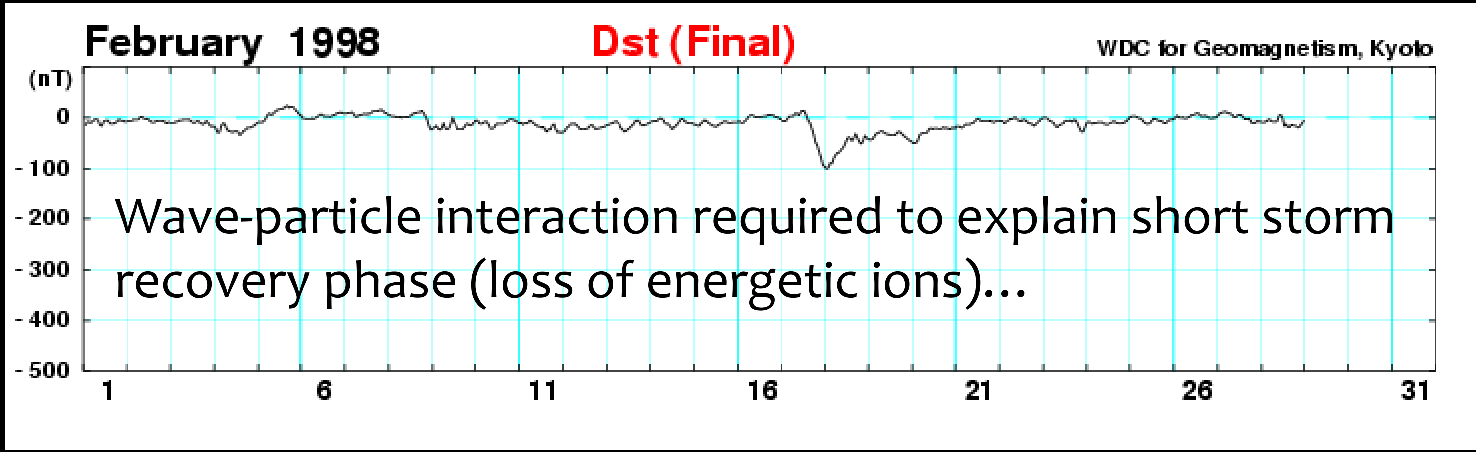

Ring current

… and relativistic electron flux variability during different storms

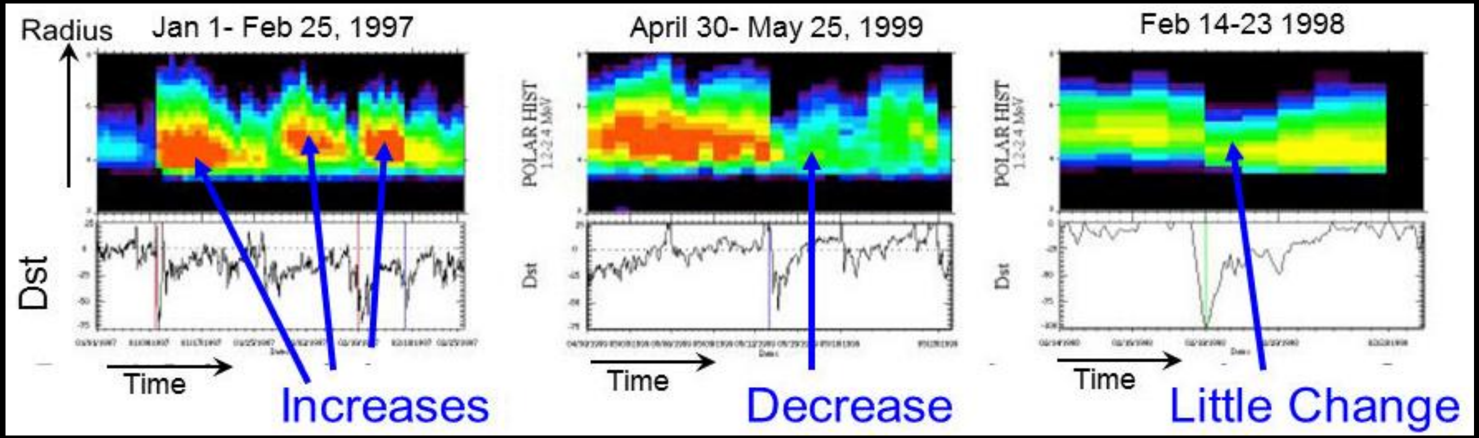

Radiation belts

Reeves et al., 2003

Energy dependence

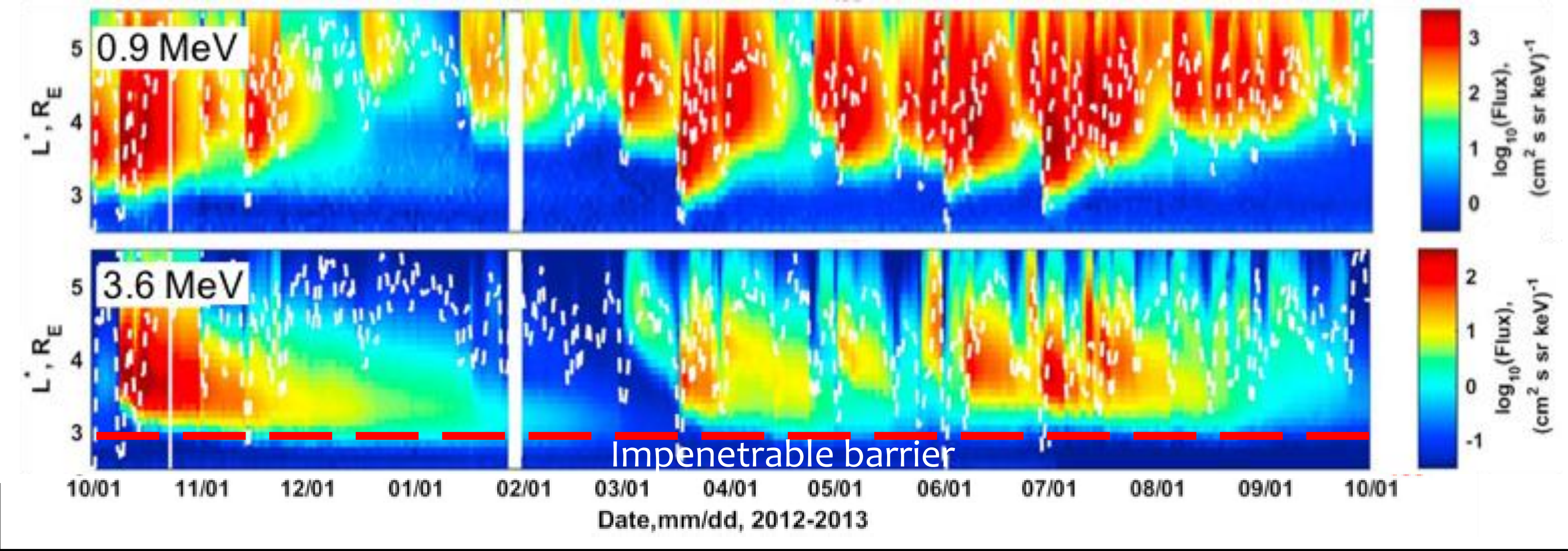

~MeV and ~a few MeV electron fluxes exhibit different behavior (Drozdov et al., 2015)

Multi-MeV electrons do not penetrate inside L~2.8 (Baker et al., 2014)

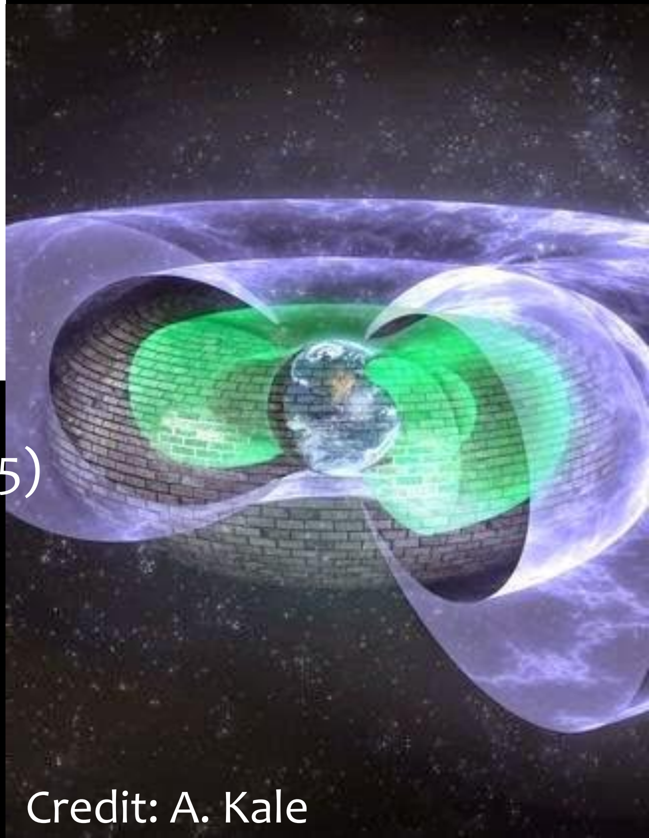

Credit: A. Kale

Effect on the plasmasphere

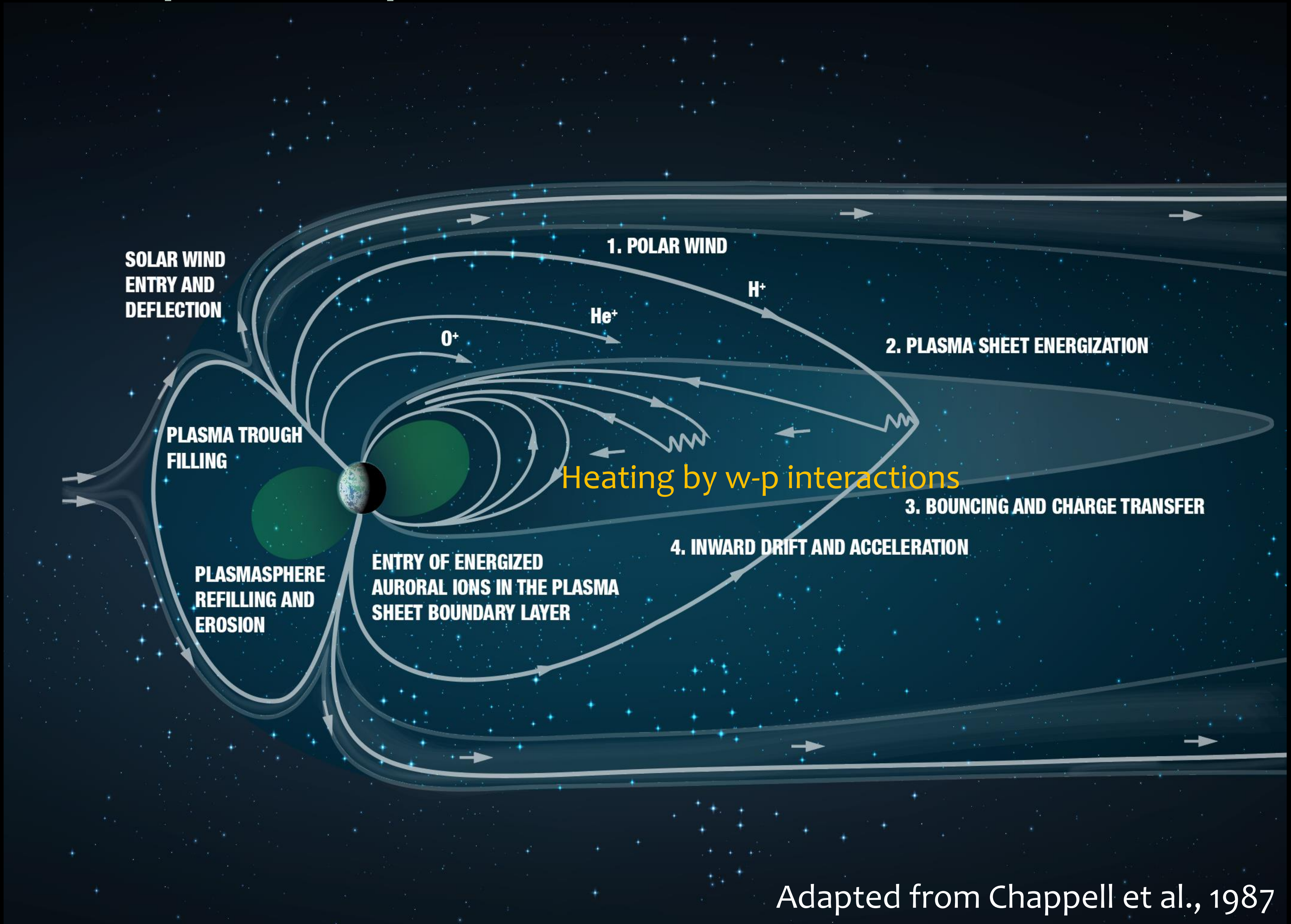

Adapted from Chappell et al., 1987

What happens in the inner magnetosphere region?
How do electrons and ions get energized and lost?

Periodic charged particle motion

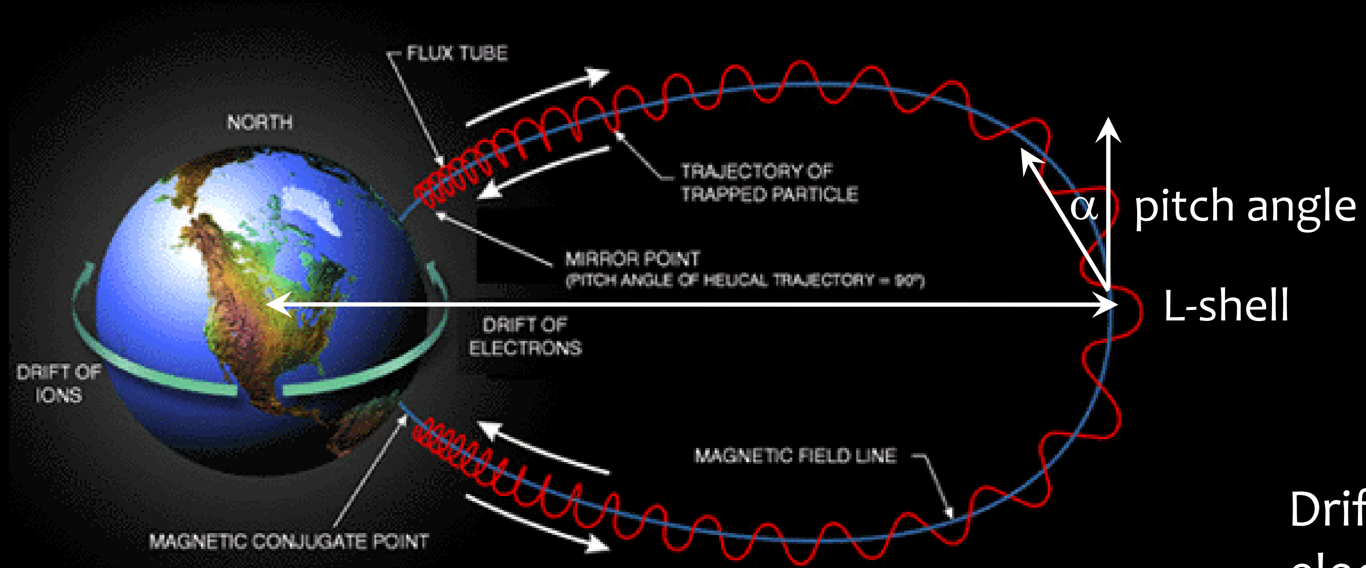

Cyclotron motion
electrons ~kHz
protons ~1-10Hz

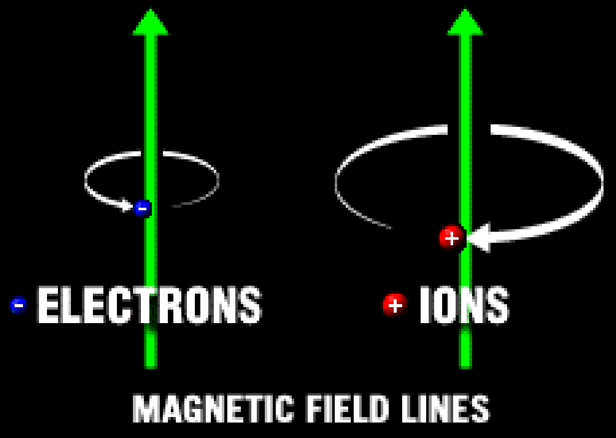

Bounce motion
1MeV electrons
@ GEO~1Hz

Drift motion
electrons ~mHz

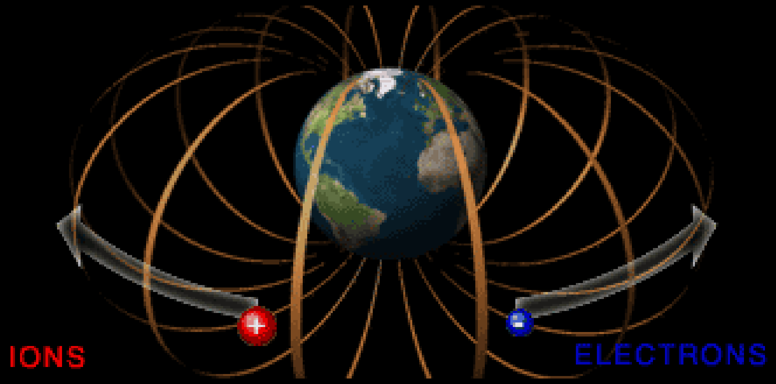

Periodic charged particle motion cont'd

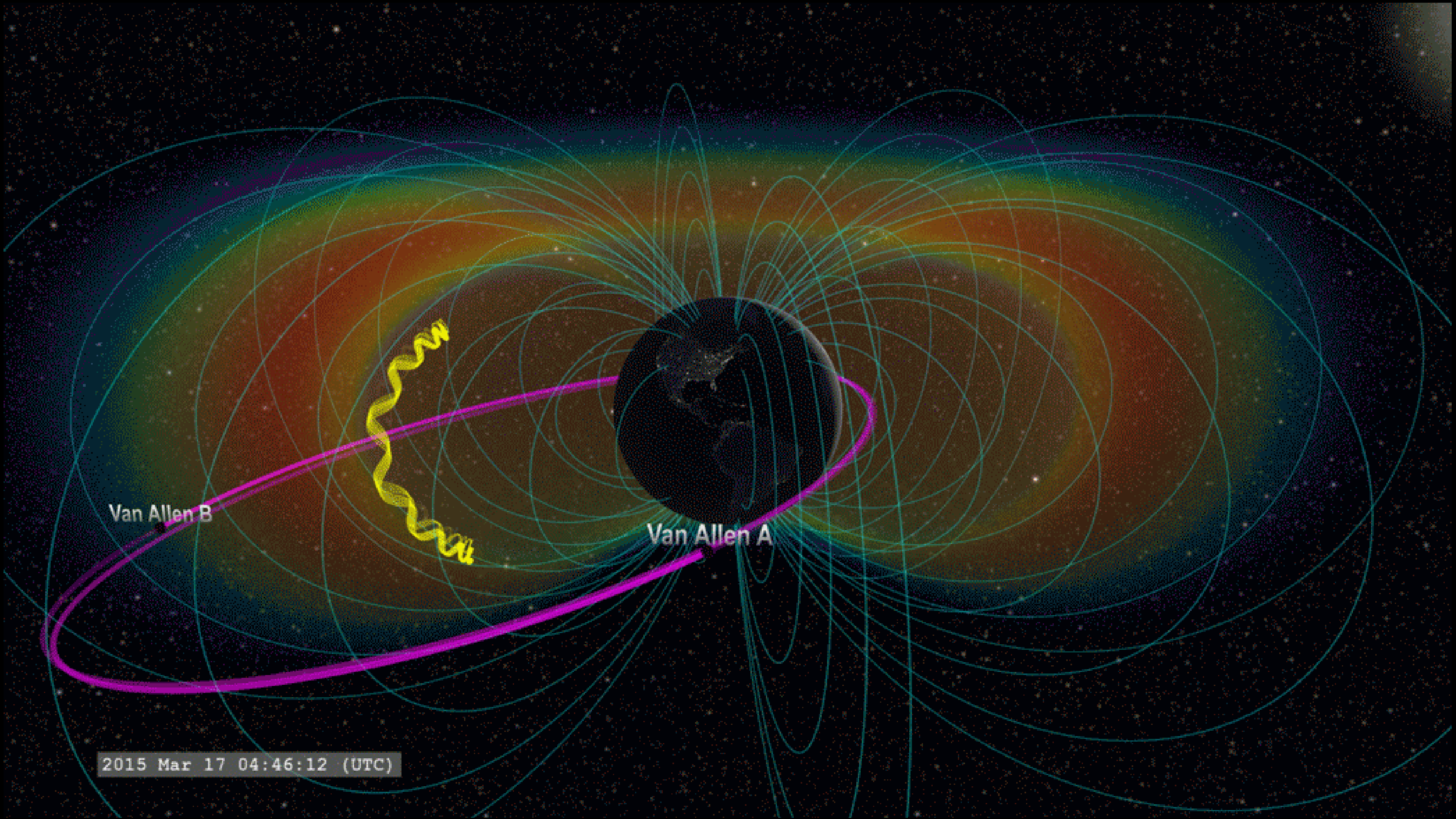

Characteristic timescales

Wave-particle interactions are associated with violation of adiabatic invariants – see the timescales as a function of L and energy on the right.

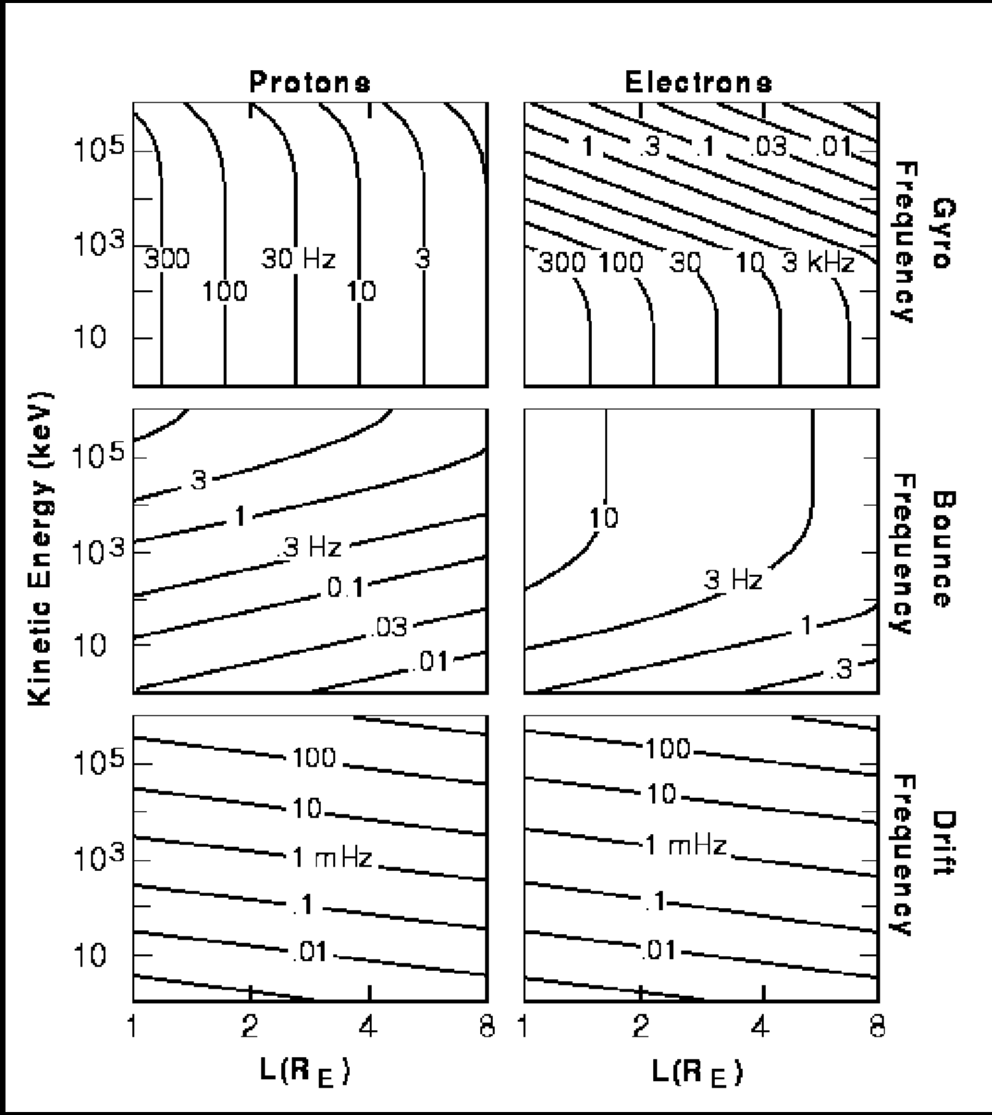

Schulz and Lanzerotti, 1974

Ultra low frequency (ULF) waves: ~mHz – a few Hz

Solar wind impulses on the dayside

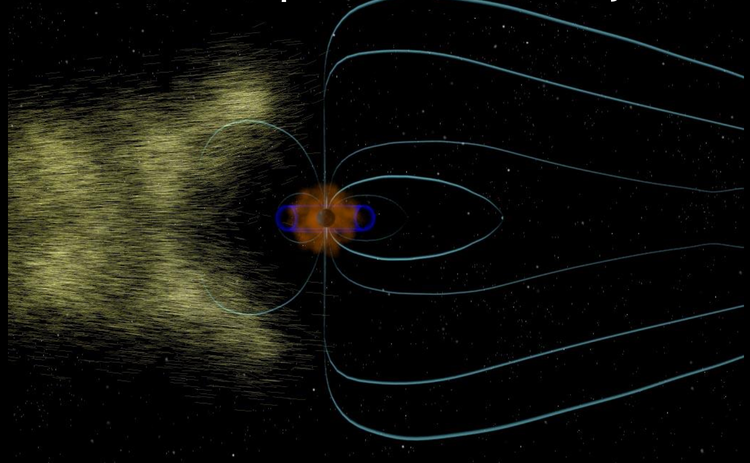

Kelvin-Helmholtz "wind-over-water" instability on the flanks

Plasma instabilities and fast flows on the night side

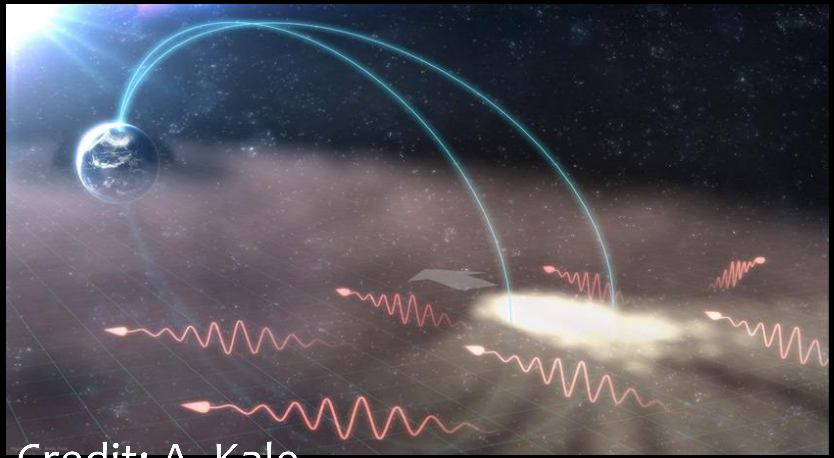

Credit: A. Kale

EMIC waves traditionally classified as ULF waves based on their frequency but they are generated on a microscopic scale

ULF wave classification

- Geomagnetic pulsations or ultra-low-frequency (ULF) waves cover roughly the frequency range from 1 mHz to 1 Hz
- Largest wavelengths and lowest frequencies in system
- Amplitudes ~few nT in B, and ~few mV/m in E

Pulsation classes						
Continuous					Irregular	
Pc1	Pc2	Pc3	Pc4	Pc5	Pi1	Pi2
0.2-5s	5-10s	10-45s	45-150s	150-600s	1-40s	40-150s
0.2-5Hz	0.1-0.2Hz	22-100mHz	7-22mHz	2-7mHz	0.025-1Hz	2-25mHz

ULF wave classification according to type and period (Jacobs, et al., 1964)

EMIC waves which are observed on the ground are referred to as Pc1-2 pulsations

Spectrogram/sonogram from CARISMA ground station

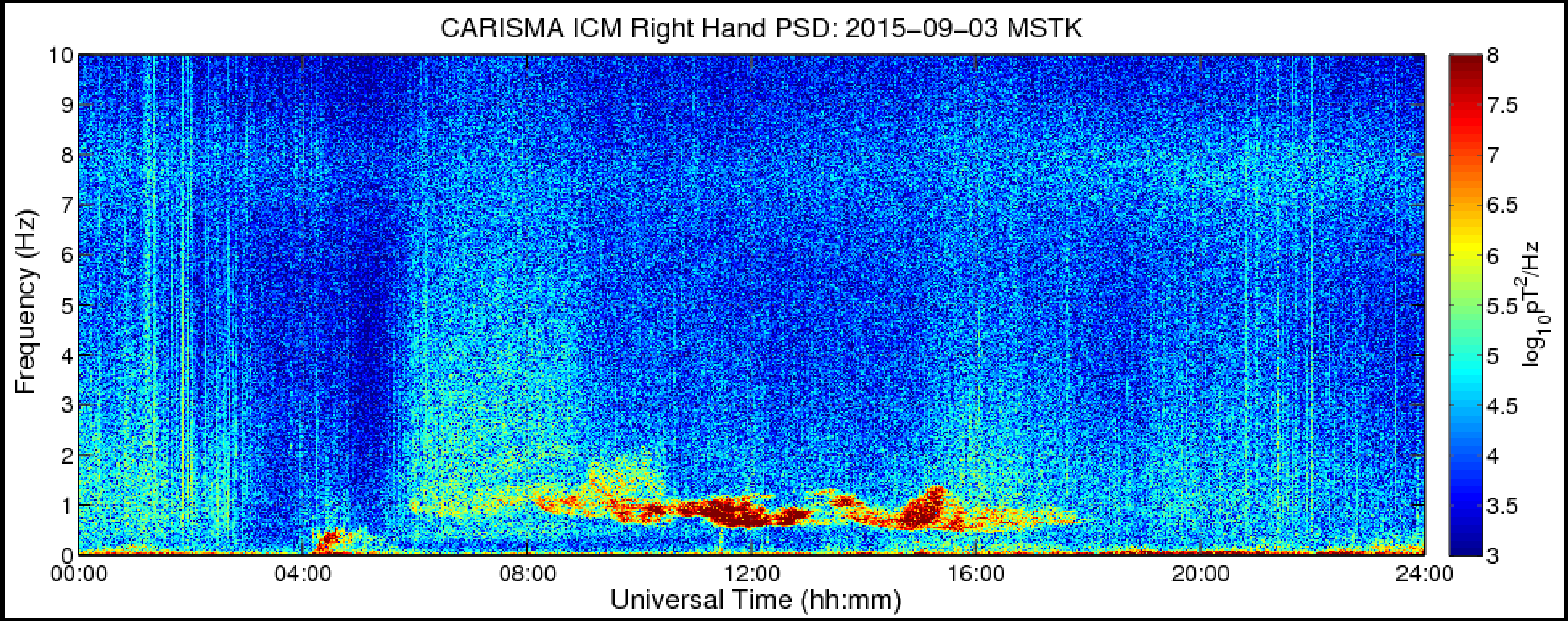

- On the ground, EMIC waves are seen as structured emissions and IPDP (Intervals of Pulsations with Diminishing Periods)
- Structured Pc1-2 pulsations are characterized by slow variations in frequency
- IPDPs exhibit fast frequency fluctuations on a timescale of tens of minutes
- IPDP events are usually short-lived and localized (~1 hour; ~3 hours Clilverd et al., 2015)
- Structured Pc1-2 events can span several hours of local time (Usanova et at., 2014; Engebretson et al., 2015)

EMIC (electromagnetic ion cyclotron) waves

- Transverse plasma waves generated by wave-particle interaction (ion cyclotron instability)
- Energy source: 10 - 100 keV protons with $T_{\perp} > T_{||}$
- Amplitudes in space:
  ~1 nT in B, ~1 mV/m in E

- Multiple bands, typically H^+, He^+,O^+
- Other bands: He^{++} (Engebretson et al., 2018); N^+ (Bashir and Ilie, 2018)

- Instability parameter: $\Sigma_h = A_h \beta_{||h}^{\alpha_h}$, $A_h = {}^{T_{\perp h}}/_{T_{||h}} - 1$,
  $\beta_{||h} = 2\mu_0 n_h k T_{||}/B^2$, $\alpha_h = \alpha_0 - \alpha_1 \ln\left(\frac{n_h}{n_e}\right) - \alpha_2 \left[\ln(\frac{n_h}{n_e})\right]^2$

→ the most unstable regions combine large A_h and large $\beta_{\|h}$ with large n_e (Blum et al., 2009; Denton et al., 2014)

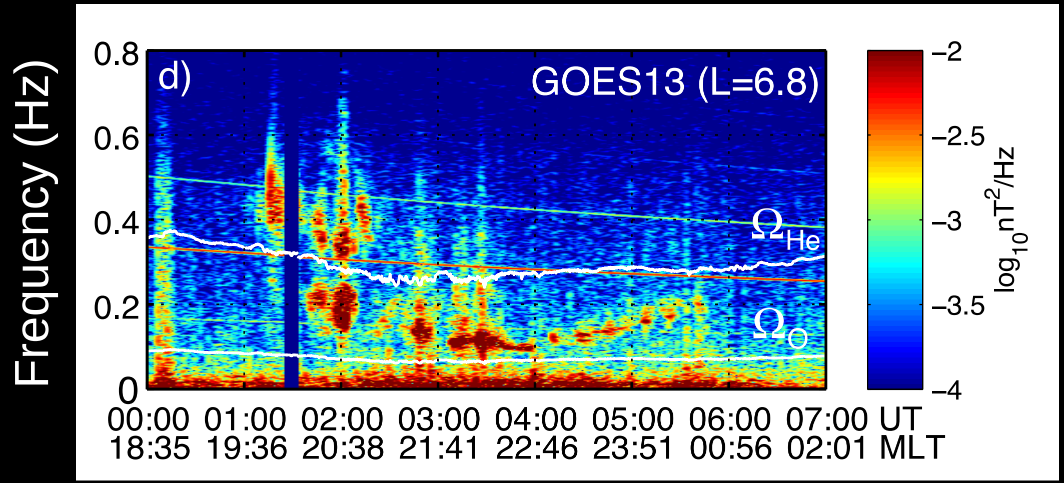

Geosynchronous magnetic field measurements. Usanova et al., 2016

Drift paths of electrons and ions in the magnetosphere

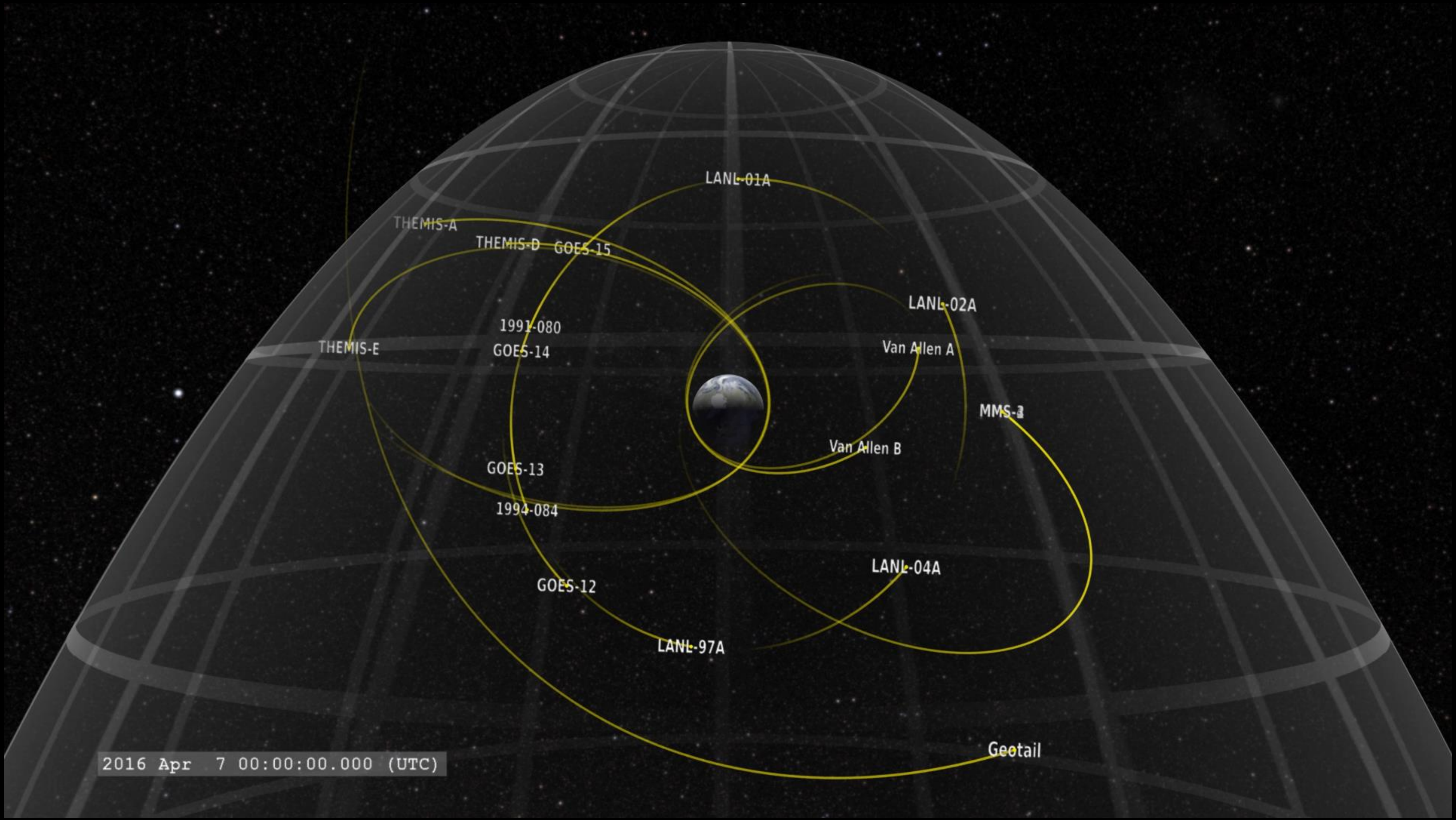

Sources of anisotropy

- EMIC waves can be observed anywhere along the ion drift path
- Convection electric field can generate ion anisotropy as particles are transported from the tail radially inward conserving their first and second adiabatic invariants
- <10 keV ions can drift along the dawn side
- Compressions can generate EMIC waves through:
    - Adiabatic heating (bursty type)
    - Drift-shell splitting (continuous type)
    - Shabansky orbits (continuous type)

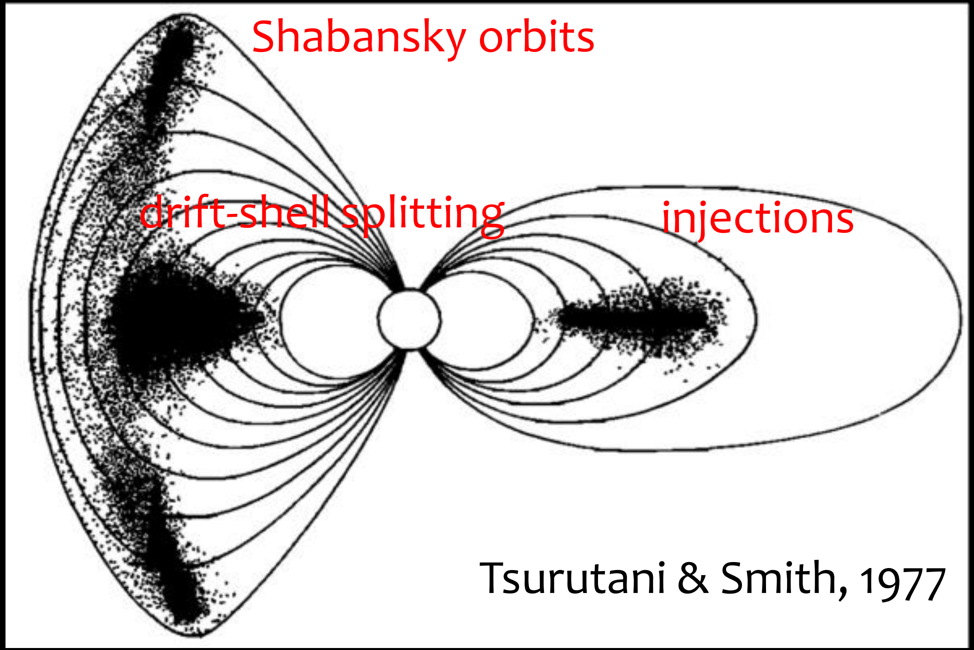

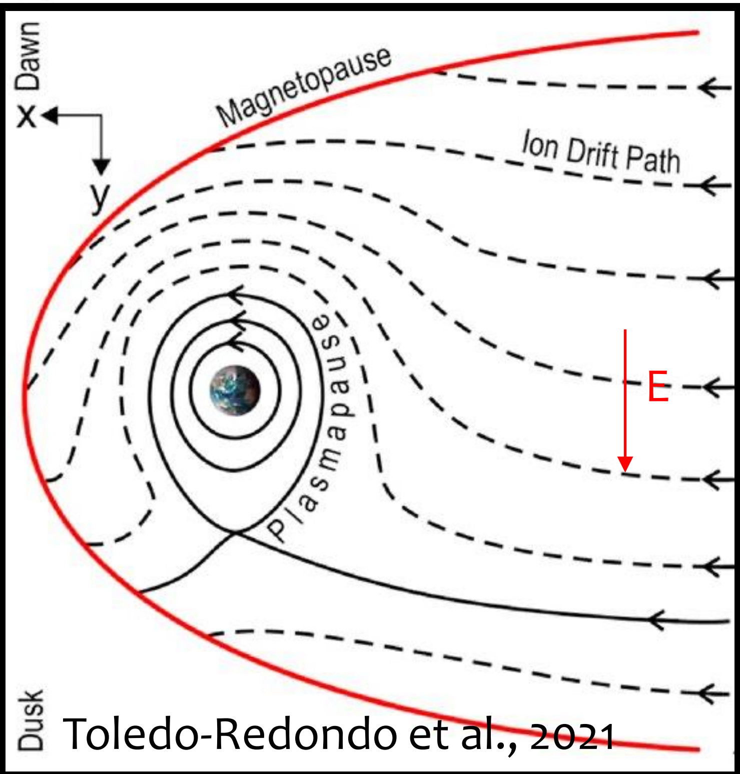

Physical mechanisms of compression events

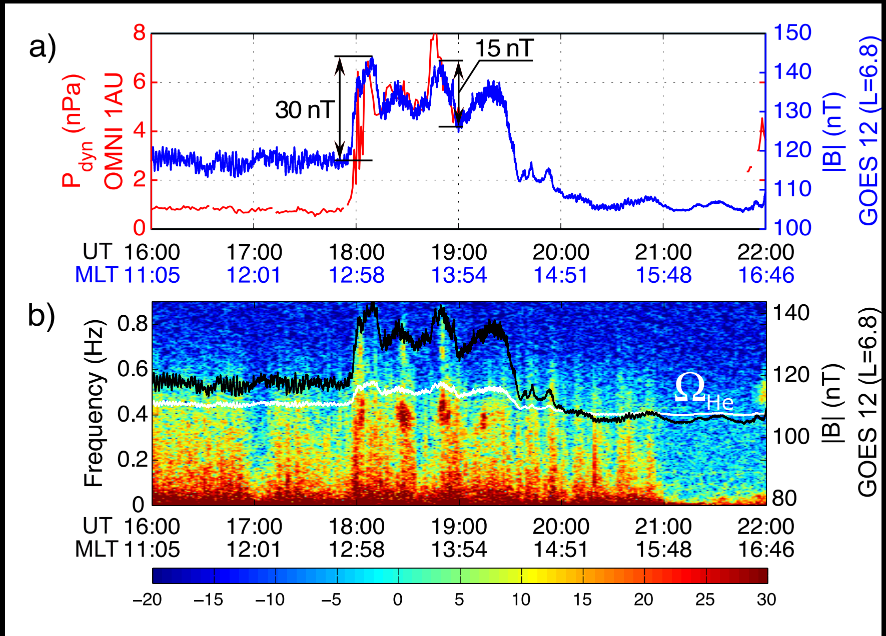

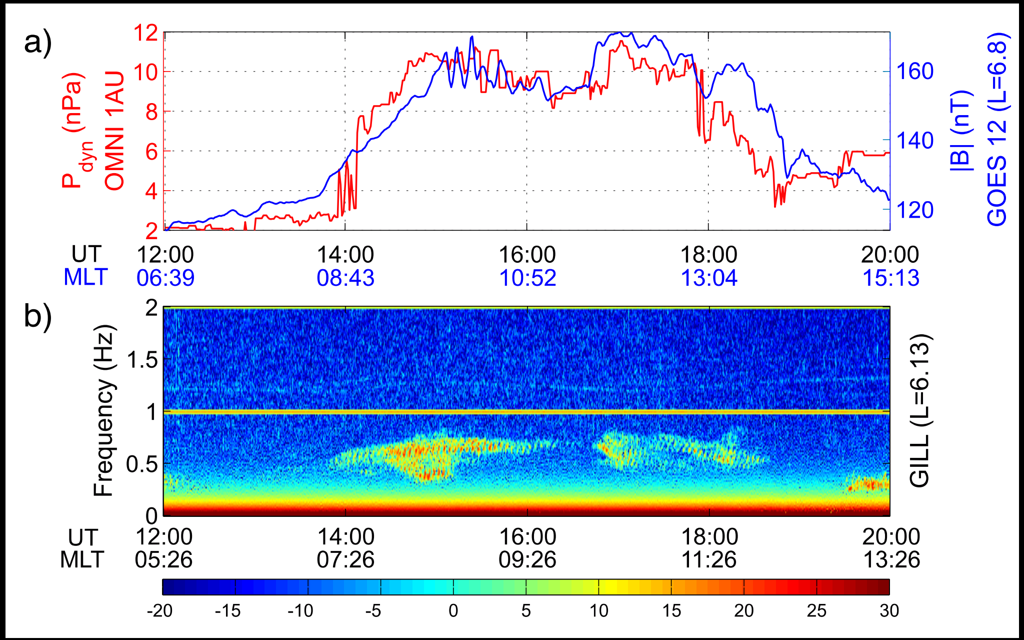

$$A = \frac{B^{1/3}}{B_0}(A_0 + 1) - 1$$

See next slide

Short-term compressions increase $T_\perp/T_\parallel$ through adiabatic heating and can generate EMIC wave bursts during periods within which the magnetic field strength is increasing (Olson and Lee, 1983)

Physical mechanisms: continuous events

Drift shell splitting

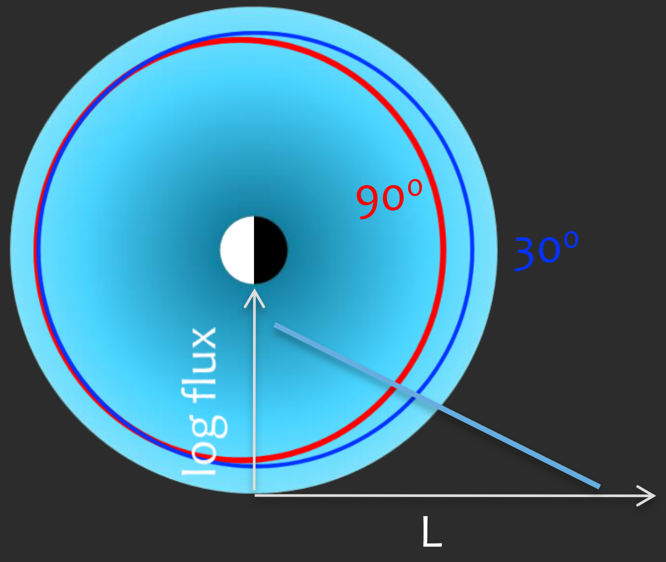

In a compressed magnetic field 90⁰ pitch angle particles follow lines of constant B, and particles with smaller pitch-angles move along more circular orbits.

The 90⁰ pitch-angle particles have a larger PSD. This makes the distribution anisotropic with $T_{\perp} > T_{\parallel}$

Shabansky orbits

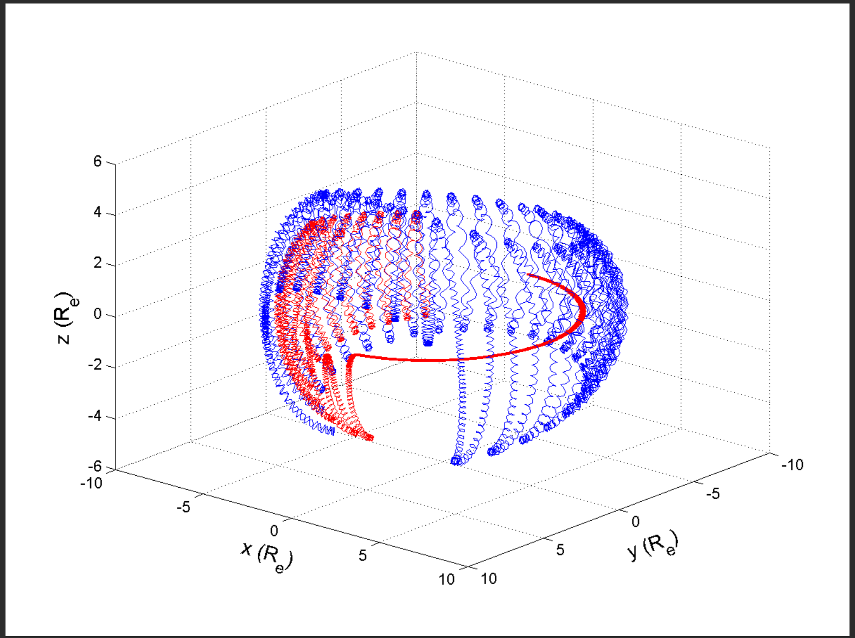

Close to the magnetopause, a compressed magnetic field can have B_{min} regions located off the equator.

McCollough et al., 2010: in Shabansky regions particle distributions gain anisotropy due to a particle's pitch-angle shifting towards higher pitch-angles.

Cyclotron, Landau and bounce resonances

EMIC waves can interact resonantly with ions and electrons if Doppler-shifted wave frequency (in the frame of reference of the particle) matches the particle cyclotron frequency:

$$\omega - k_{\|} v_{\|} = n\Omega/\gamma \, , n = 0, \pm 1, \ldots$$

$k_{||}$ is the the wave number and $v_{||}$ is the particle velocity parallel to the background magnetic field (Horne and Thorne, 1998; Summers et al., 2007).

Cyclotron resonance with energetic electrons and ions does not change particle energy, only resulting in scattering (momentum exchange) without energy coupling.

Landau resonance $\omega = k_{||} v_{||}$ is most significant for highly-oblique EMIC waves (Thorne and Horne, 1992).

Landau interactions lead to wave attenuation and energy transfer to ~eV-ten's eV cold/thermal electrons and ~keV ions and also contribute to scattering of relativistic electrons (Cornwall et al., 1971; Omura et al., 1985; Kitamura et al., 2018; Wang et al., 2016).

Bounce resonance interactions with energetic electrons can cause particle scattering (Cao et al., 2017; Blum et al., 2019).

These resonant interactions take place when the electron bounce period (or integer number of such periods) matches the wave period.

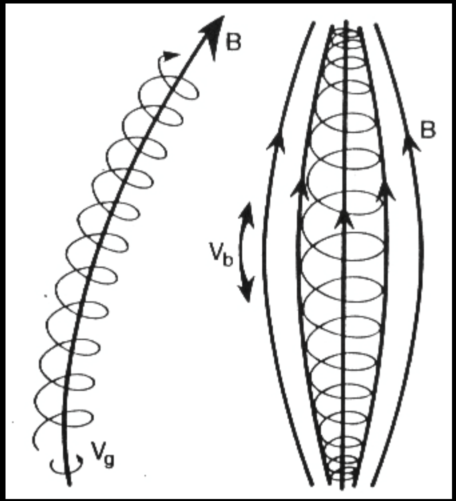

Cyclotron wave generation

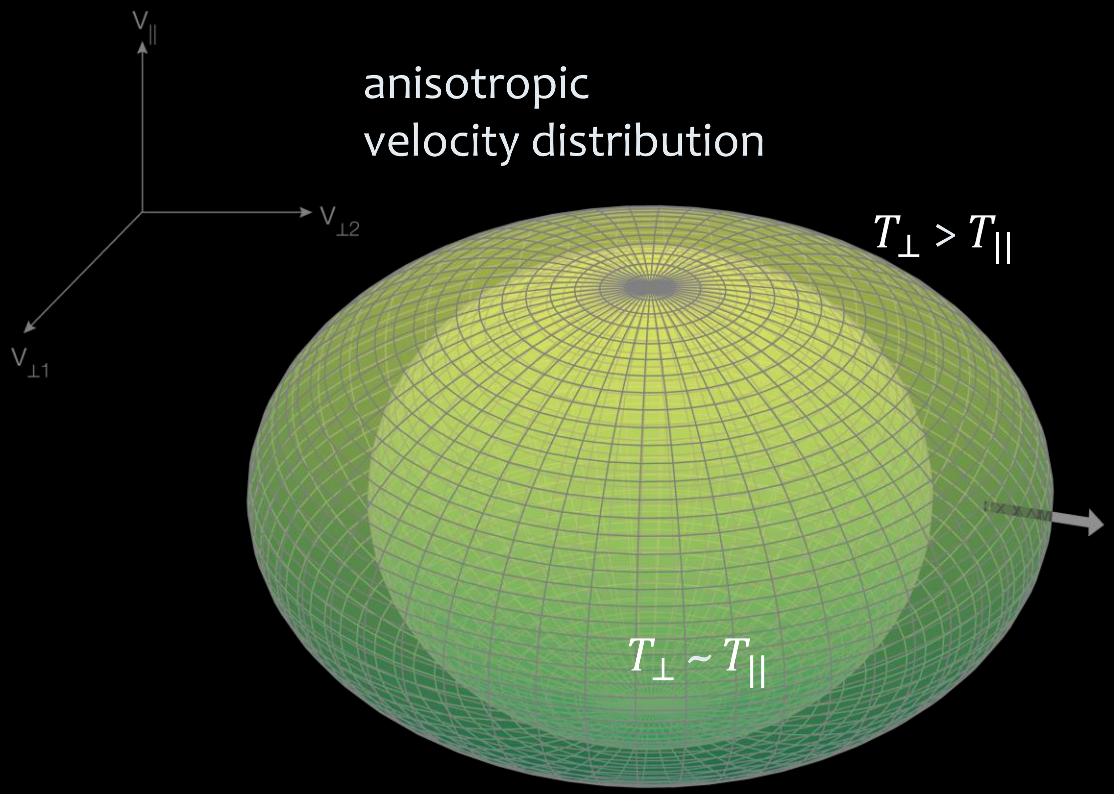

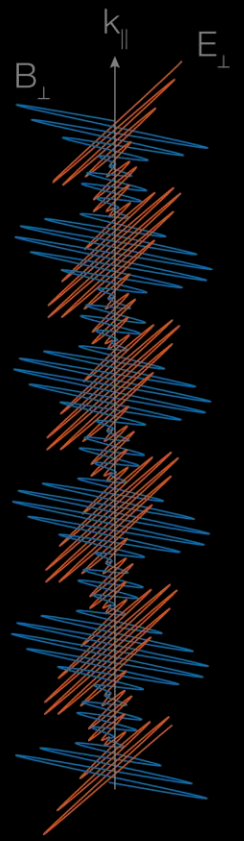

+ thermal particle heating
e.g., He+ (Kitamura at al., 2018)

This mechanism works in a similar way
for electron and ion cyclotron waves

Cyclotron wave
Right-hand polarization for electrons
Left-hand polarization for ions

Heating of thermal He^+

Parameters from GEOS satellite at L~7
B=140 nT
Isotropic cold H^+ n=10cm^{-3}
Isotropic cold He^+ n=2cm^{-3}
$E_{H+}=E_{He+}$=1.7 eV
Hot H+ n=1.1 cm^{-3}
$E_{||H+}$=17 keV
$T_\perp / T_{||}=2$

Omura et al., 1985

Hybrid code: electrons as massless fluid, ions as particles (x, Vx, Vy, Vz)

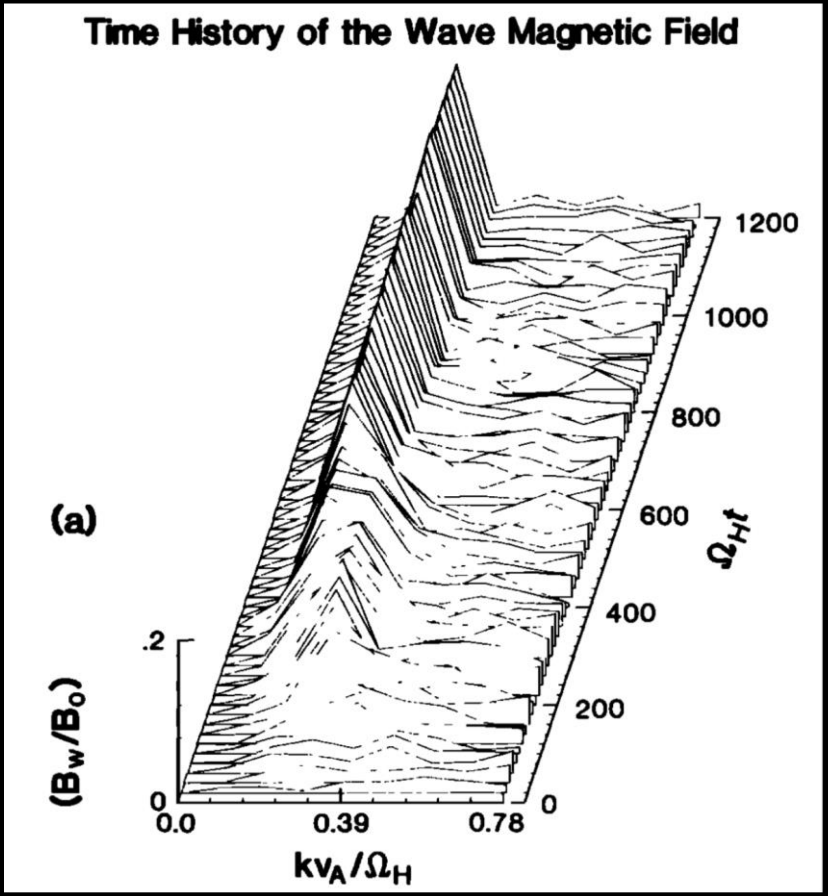

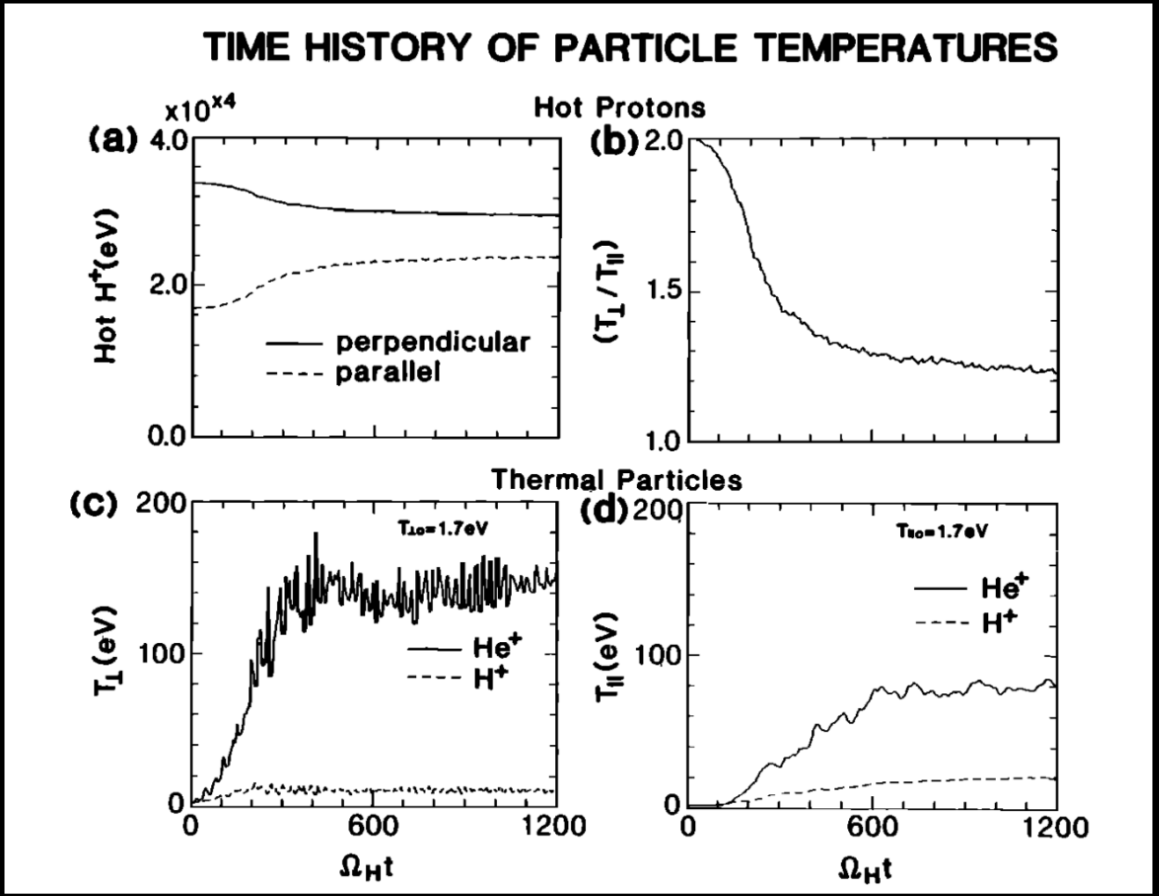

Non-linear structure

T=0 He+ ions are uniformly distributed in phase space
T=100 perturbations in V_y from $E_w x B_0$
T=300 perturbation in V_x from $dV_{y,z} x dB_{z,y}$
T=400 nonlinear motion
Plasma mixing results in hotter distributions (~100 times)

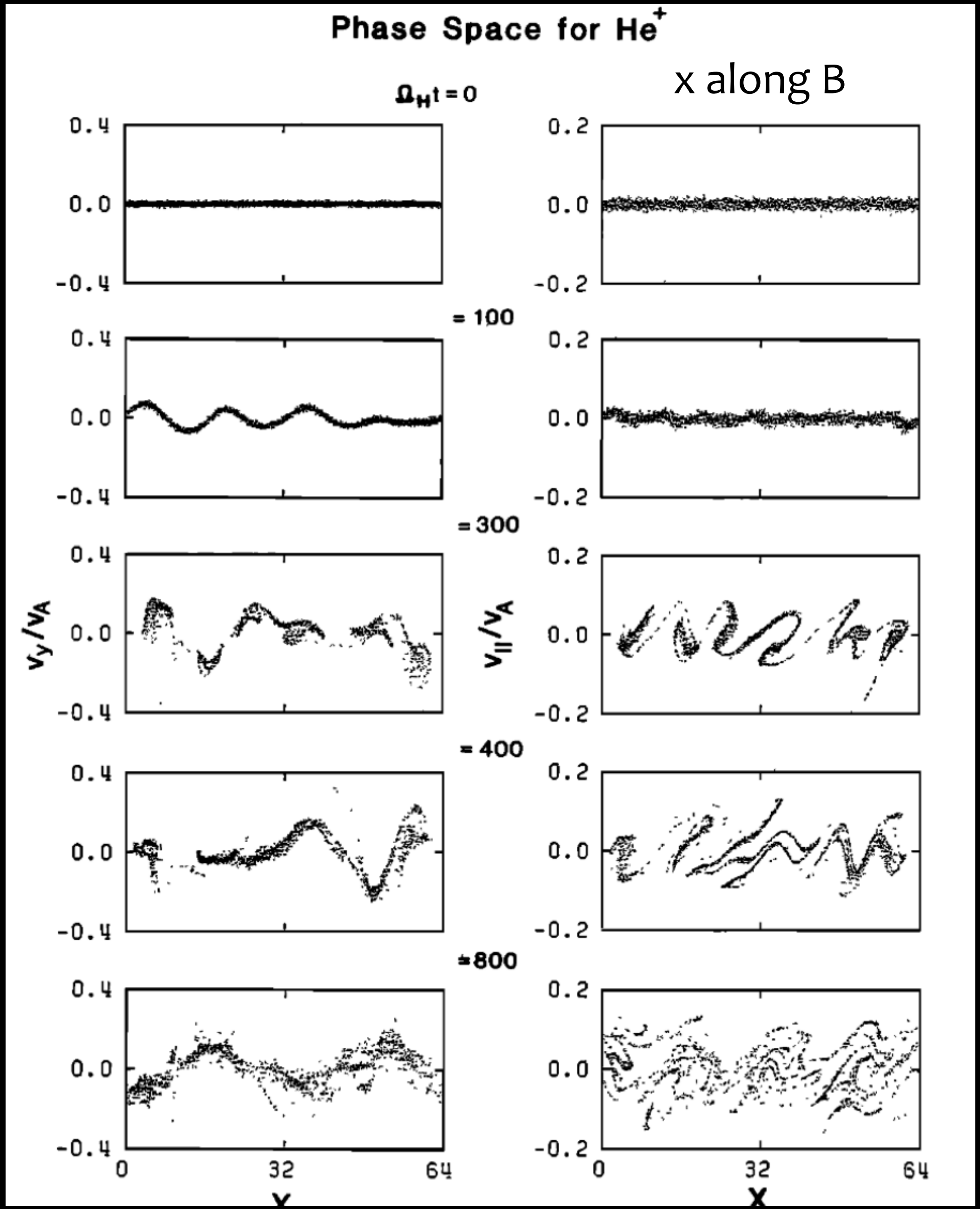

EMIC waves, proton aurora and electron precipitation

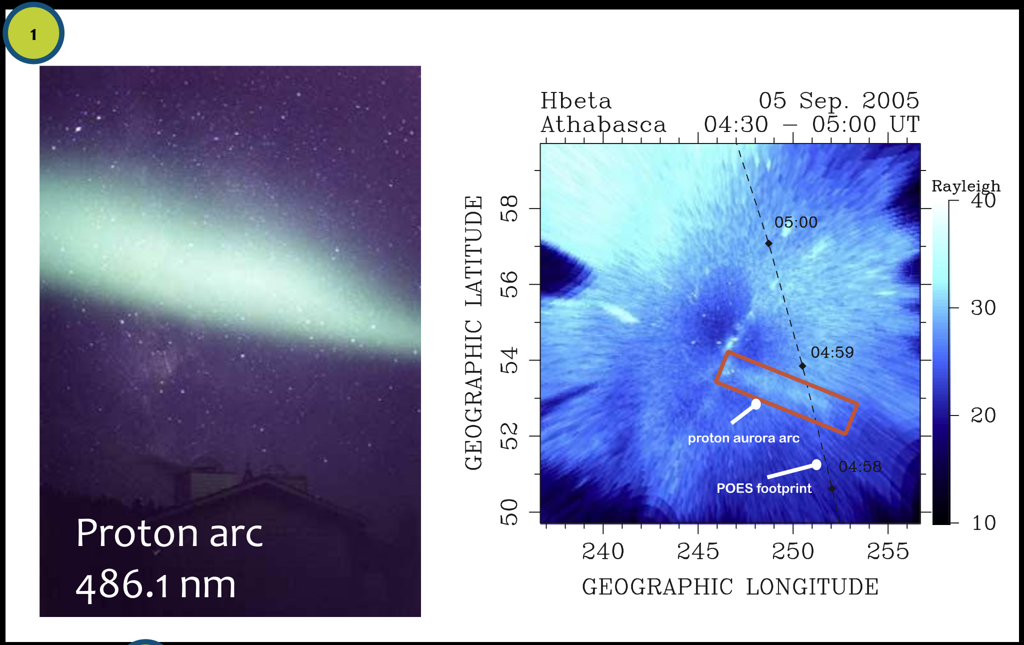

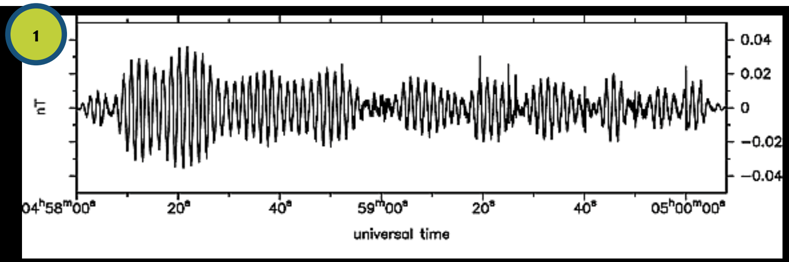

He-band EMIC waves on the ground

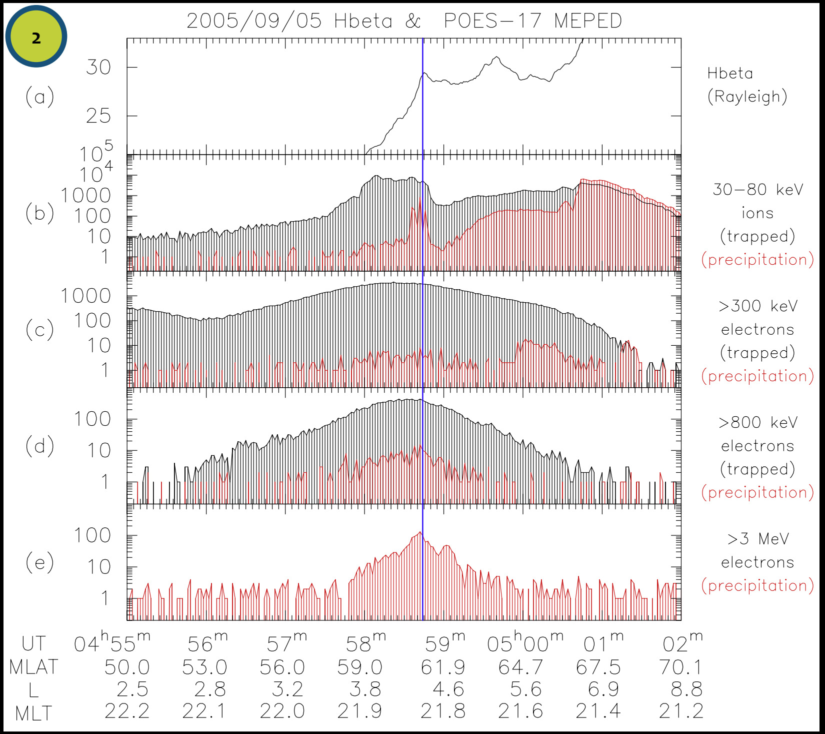

Precipitating protons and electrons at LEO
Miyoshi et al., 2008

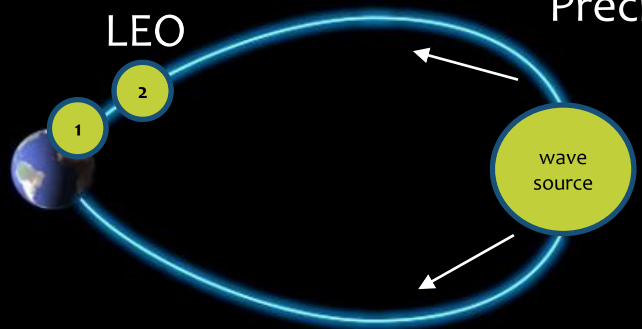

EMIC wave activity and duskside energetic electron precipitation

(a) BARREL balloon 1C observations, (b) GOES 13 wave measurements, (c–e) solar wind conditions, and (f and g) geomagnetic AE and SYM-H indices on 18–19 January 2013. The red vertical dashed lines mark the sudden enhancements in the solar wind dynamic pressure and the purple dashed lines and shaded regions the times of relativistic electron precipitation.

Concurrent wave and precipitation measurements support the theoretical picture of duskside interaction between EMIC waves and MeV electrons leading to precipitation.

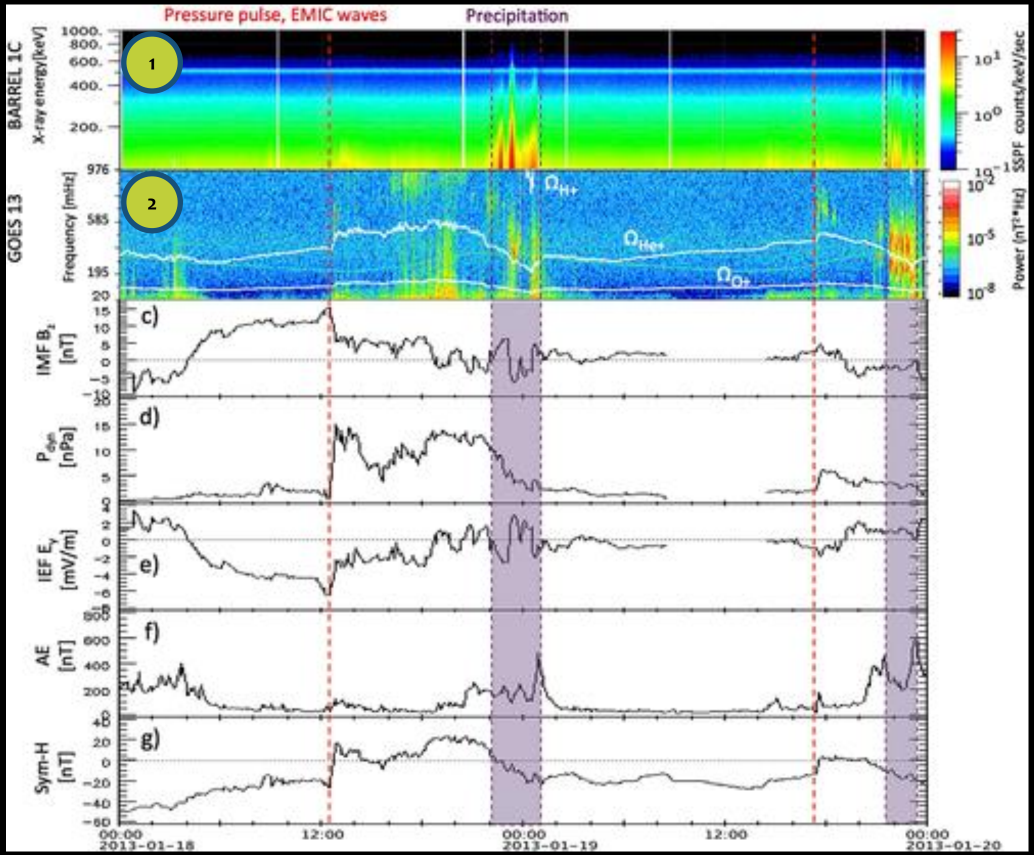

Blum et al., 2015

Bremsstrahlung X-rays measured by BARREL

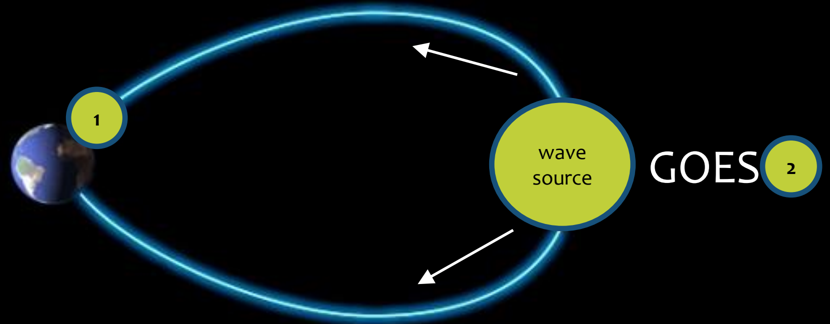

Dispersion relation and electron resonance energy: cold plasma approximation ($\beta \ll 1$)

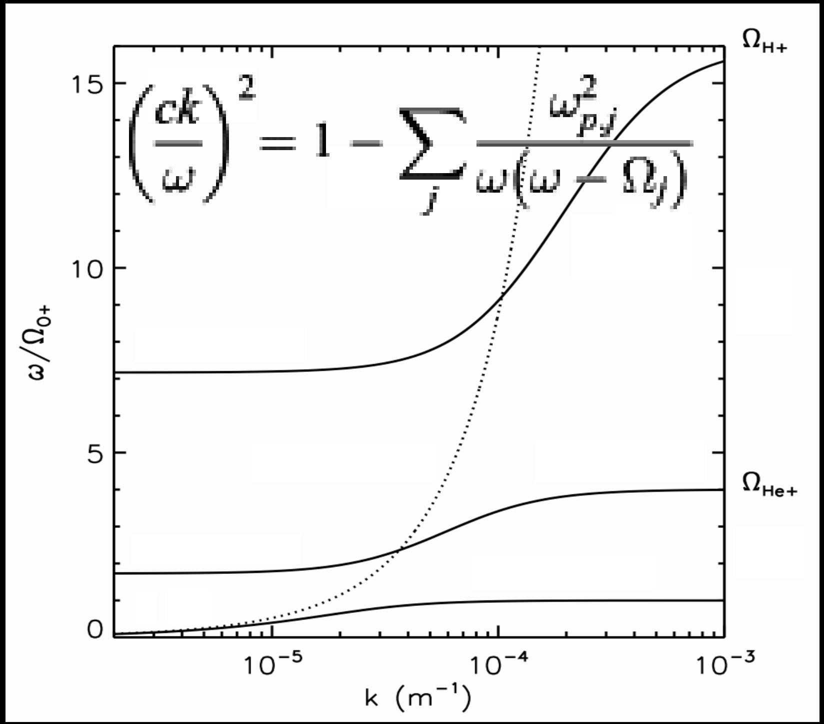

Adapted from Thorne et al., 2006

- Parallel propagation
- 70% H+, 20% He+, and 10% O+
- Solid curves: H+, He+, and O+ ion modes
- Dashed curve: electron mode

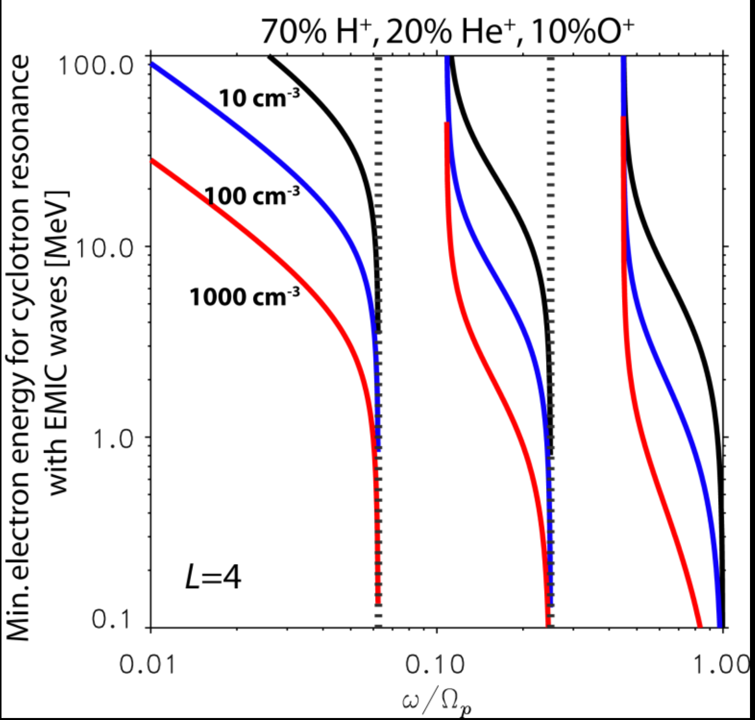

Ukhorskiy et al., 2010

Minimum electron resonance energy for parallel propagating LH-modes with different plasma densities

Kinetic dispersion relation

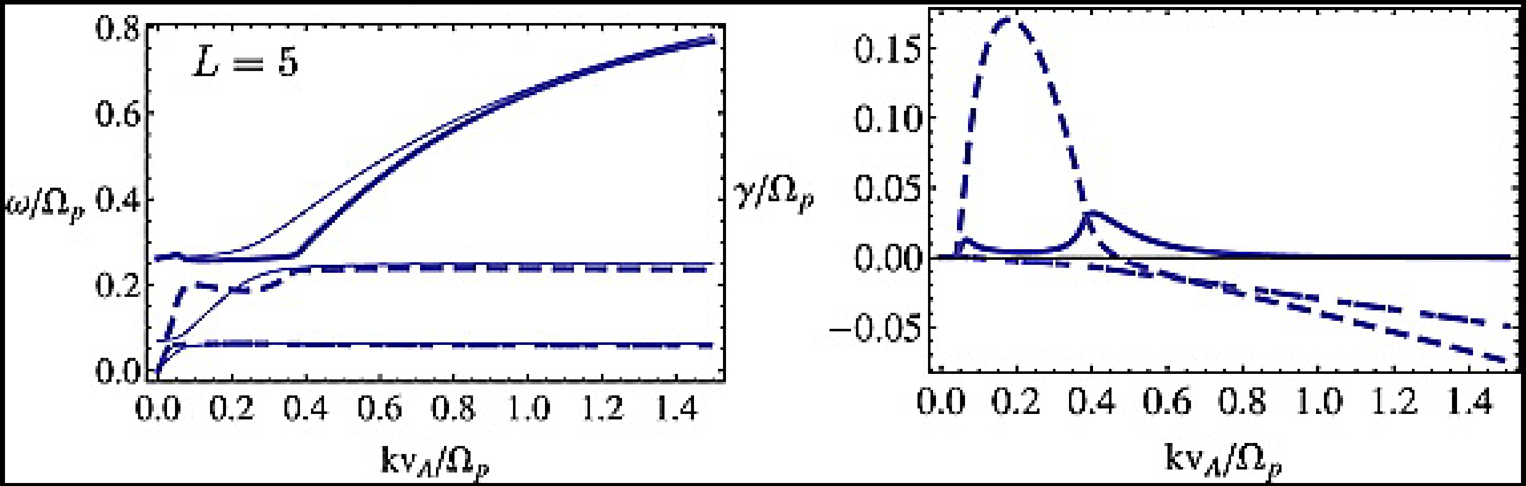

Silin et al., 2011

$$\Omega^2 = c^2k^2 - \sum_j \omega_{pj}^2 \left(A_j - \left((A_j + 1)(\Omega_j - \Omega) - \Omega_j \right) \frac{Z(z_j)}{k v_{Tj}} \right)$$

Dispersion curves for EMIC waves in multi-ion plasma. (left) Real frequencies and (right) growth rates.

Thin lines correspond to the cold approximation.
Thick lines correspond to the full kinetic approach.

1. In the warm kinetic approximation EMIC waves can grow inside the stop bands
2. Kinetic effects lead to strong cyclotron damping of the EMIC waves at large wave numbers

Kinetic effects

- In a warm plasma E_{min} is controlled by k
- $E_{min} \rightarrow 0$ when $\omega \rightarrow \Omega_j$ in the cold plasma approximation appears because $k \rightarrow \infty$ as $\omega \rightarrow \Omega_j$ and there is no damping
- E_{min} does not asymptotically drop to zero at the ion gyrofrequencies
- The lowest E_{min} are achieved for largest wave numbers, but there is no clear dependence of E_{min} on wave frequency
- E_{min} is typically ~ 2 MeV. It can drop to ~0.5 MeV during plasmasphere expansion beyond L ~ 7, or inside plasmaspheric plumes
- Heavy ions decrease in resonant energies due to higher plasma mass density

Silin et al., 2011

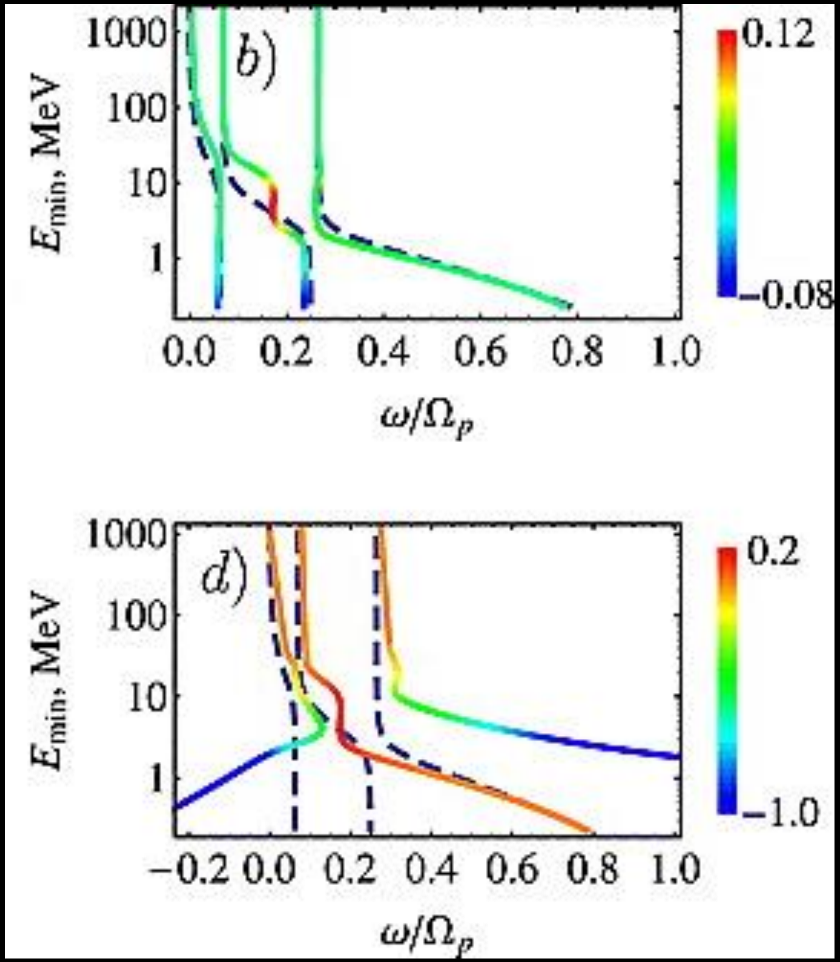

Dashed lines correspond to the cold fluid approximation
Solid lines correspond to the full kinetic approach
The color bar denotes growth/damping rates

Statistical maps

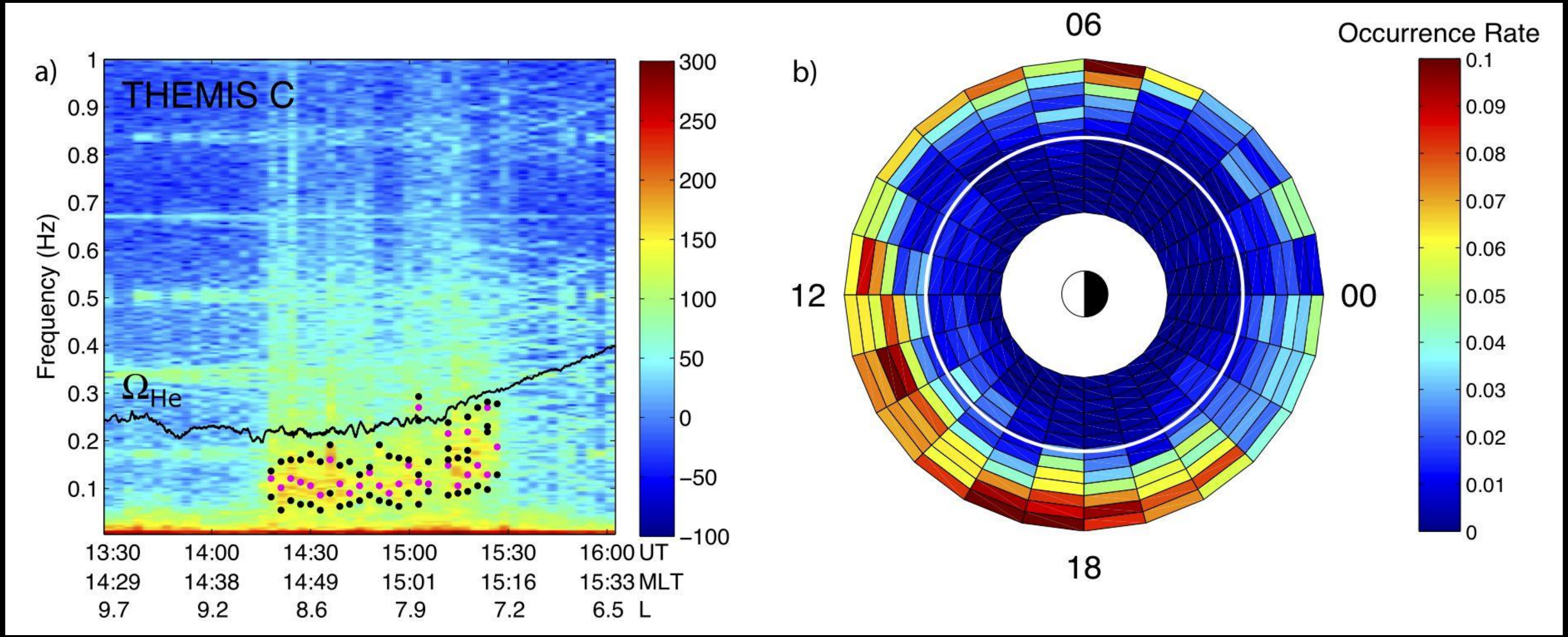

Usanova et al., 2012
THEMIS statistics 2007-2011.

EMIC occurrence in the inner magnetosphere is low.
Most wave events observed beyond GEO orbit on the dayside.

H^+ and He^+ band occurrence

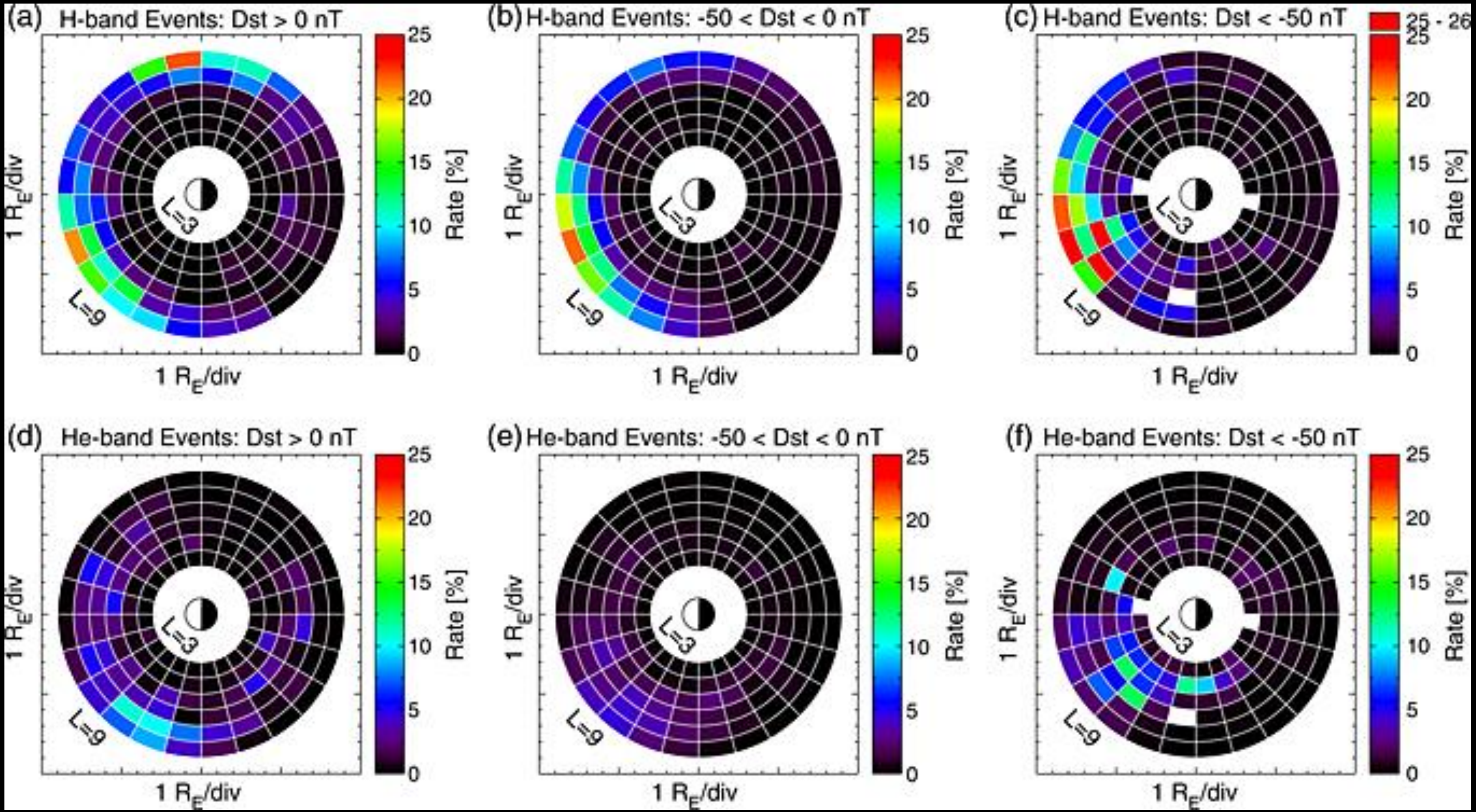

4.5 years of AMPTE/CCE data. Probability increases during compressions (positive Dst) and disturbed conditions (negative Dst).

Keika et al., 2013: He band is often excited in the inner duskside magnetosphere during storms.

Radial and local time extent

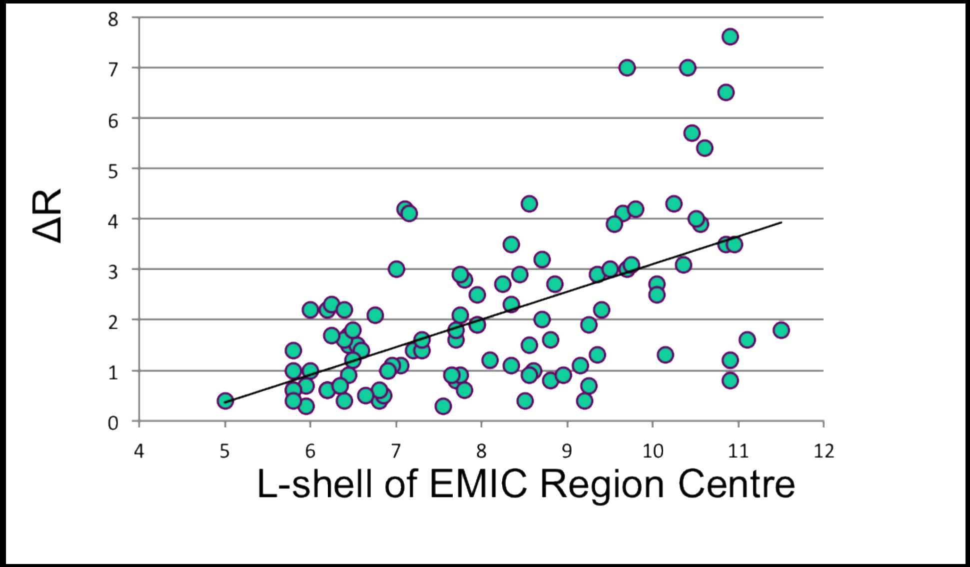

Radial width from 106 EMIC events observed on Cluster

Usanova and Mann, 2016

Information about the radial and local time extent of EMIC activity is important for estimation of energetic particle loss rates into the atmosphere.

To obtain details about both MLT and radial extent, simultaneous ground and conjugate in-situ measurements are required.

Satellite measurements provide an excellent basis for estimating the radial localization however they only offer limited capacity for estimating the MLT extent in any specific single event.

Ground observations from multiple locations around the globe offer an alternative perspective for determining the MLT extent of EMIC wave events.

However, ducting of signals in the ionospheric waveguide means that waves can be detected on the ground at long distances away from the source.

Satellite and ground distributions

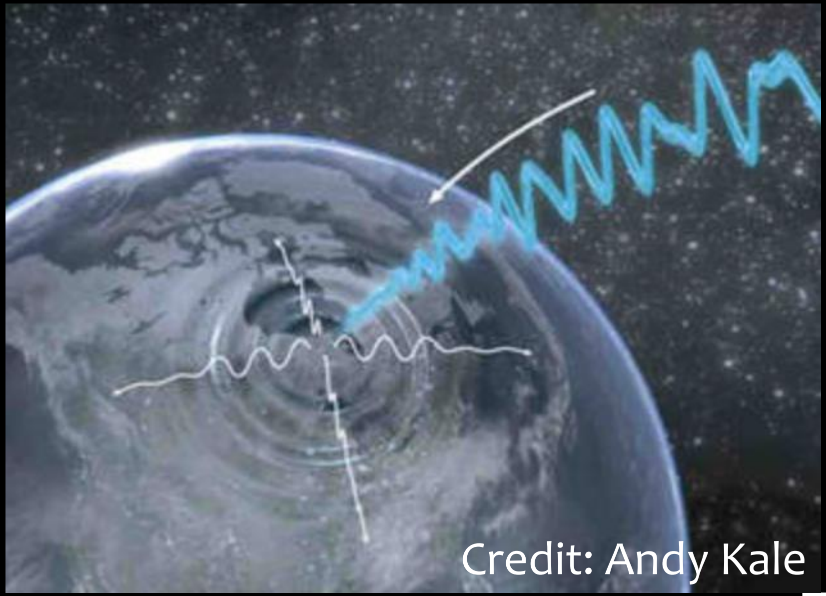

Usanova et al., AGU monograph, 2016
CARISMA and THEMIS statistics of EMIC waves occurrence 2007-2011.
Occurrence distributions look different!

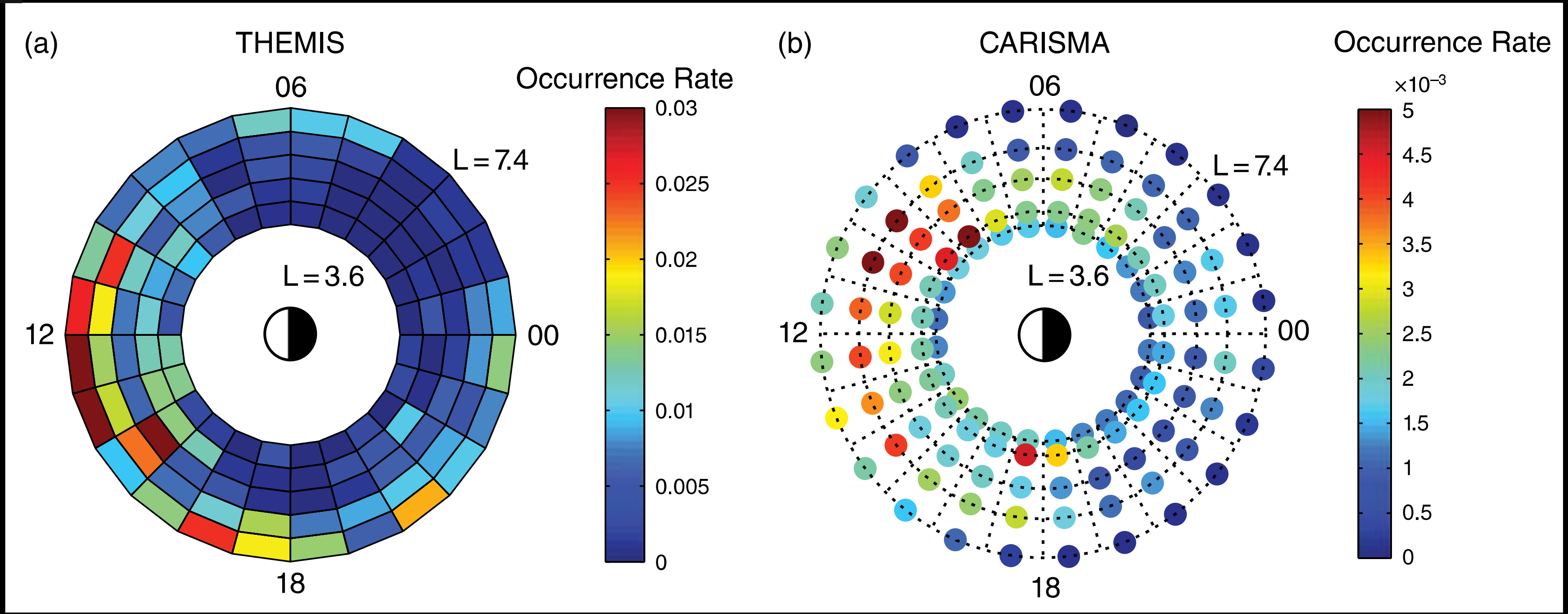

Electron pitch-angle scattering by EMIC waves

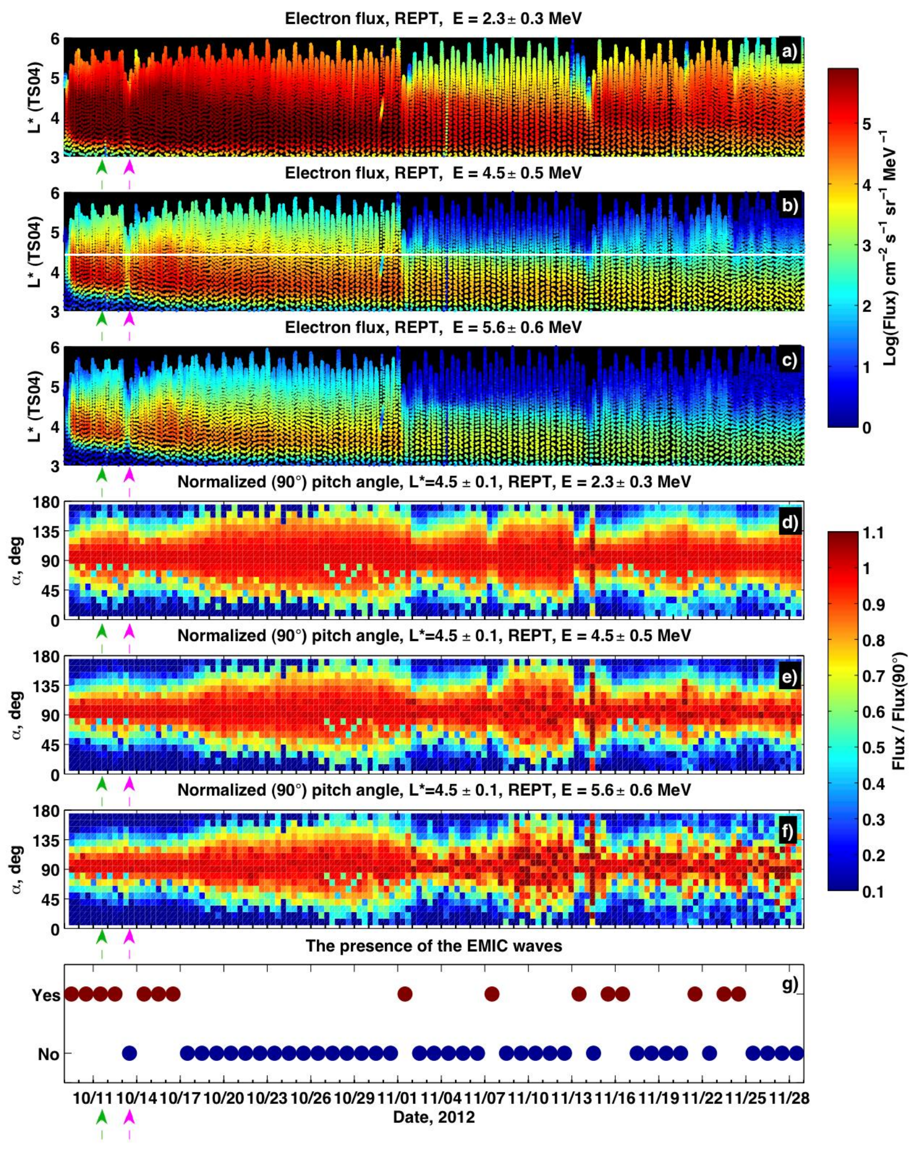

Usanova et al., 2014

- Differential electron flux as a function of L* (a-c), and normalized differential flux as a function of PA L*=4.5 (d-f) in the 2.3, 4.5, and 5.6 MeV energy channels,, and EMIC wave occurrence from L~4-4.5 on the ground from October 9 to November 29, 2012.
- EMIC waves scatter low-pitch angle particles but cannot interact with > ~45 degree pitch-angle electrons.
- Other waves modes are required to act simultaneously with EMICs to remove the core 90-degree population.

Dips in phase space density

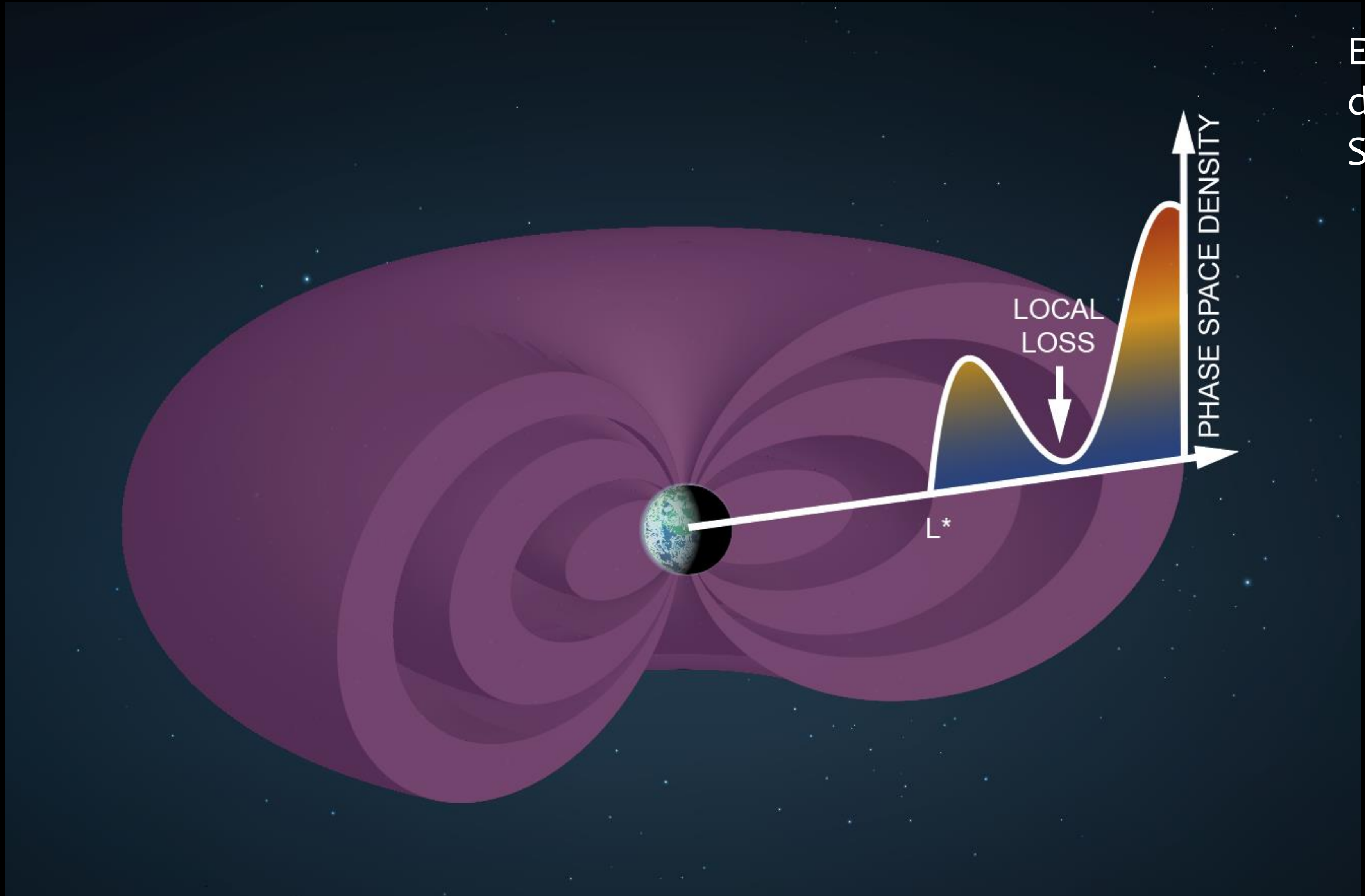

After Reeves et al., 2013

EMIC waves can cause localized dips in phase space density
Shprits et al., 2017; Aseev et al., 2017

Computed electron pitch-angle diffusion coefficients

Parameters for the electron pitch-angle diffusion estimate:
B=330 nT
n_e=150 cm^{-3}
B_{EMIC}=2 nT
f_{EMIC}=0.7-1.1 Hz – Van Allen Probes

delta MLT: 6 hours - ground

Ion composition:
70% H^+; 20% He^+; 10% O^+

Computed pitch-angle diffusion coefficients (a-c) and observed normalized electron flux as a function of pitch-angle (d-f) in the 2.3, 4.5, and 7.15 MeV for October 9-13, 2012.

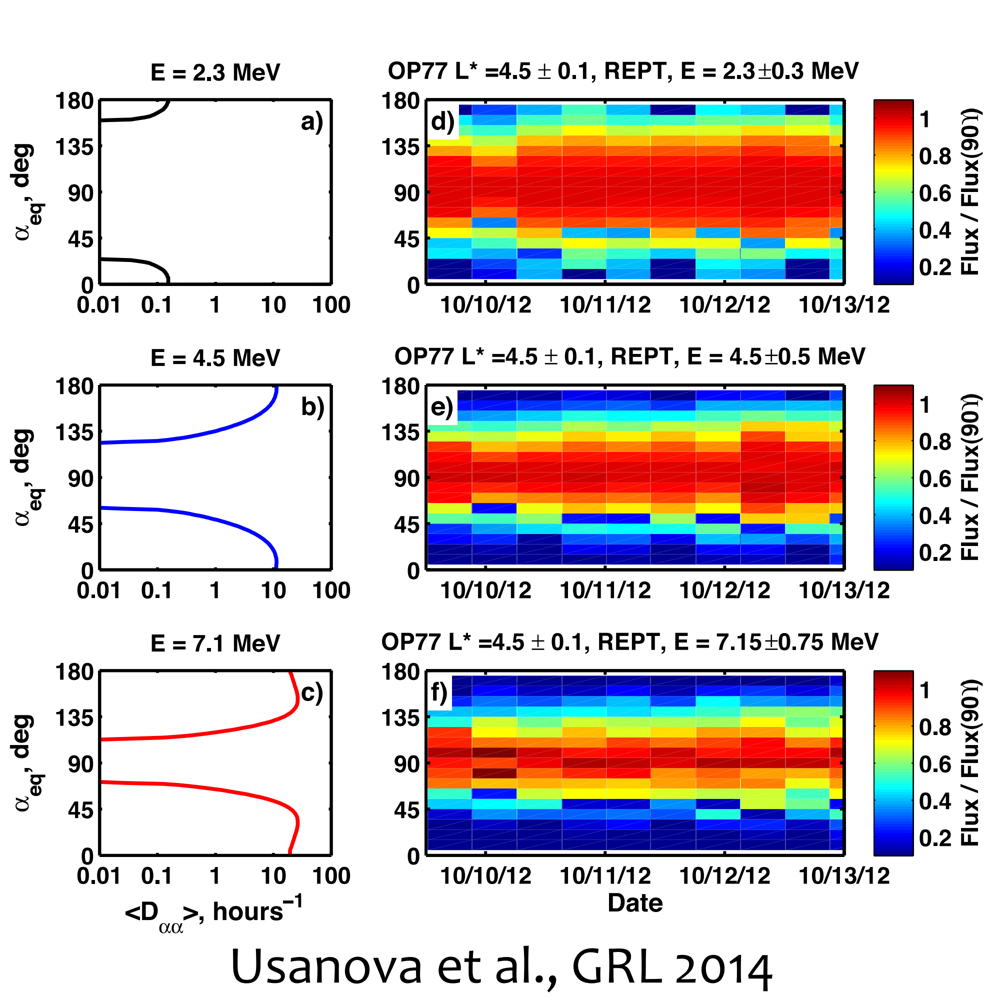

Formulation of Glauert and Horne, 2005

Diffusion models (Fokker-Planck equation)

$$
\begin{aligned}
\frac{\partial f}{\partial t}
&= L^{*2} \frac{\partial}{\partial L^*}\bigg|_{\mu,J} \left(D_{L^*L^*} L^{*-2} \frac{\partial f}{\partial L^*}\bigg|_{\mu,J} \right) \\
&+ \frac{1}{T(\alpha_0)\sin(2\alpha_0)} \frac{\partial}{\partial \alpha_0}\bigg|_{p,L^*} T(\alpha_0)\sin(2\alpha_0) \left(D_{\alpha_0\alpha_0} \frac{\partial f}{\partial \alpha_0}\bigg|_{p,L^*} + D_{p\alpha_0} \frac{\partial f}{\partial p}\bigg|_{\alpha_0,L^*} \right) \\
&+ \frac{1}{p^2} \frac{\partial}{\partial p^2}\bigg|_{\alpha_0,L^*} p^2 \left(D_{pp} \frac{\partial f}{\partial p}\bigg|_{\alpha_0,L^*} + D_{p\alpha_0} \frac{\partial f}{\partial \alpha_0}\bigg|_{p,L^*} \right) - \frac{f}{\tau}
\end{aligned}
$$

Diffusion codes: VERB (UCLA), Salambbo (ONERA), BAS-RBM (BAS), DREAM (LANL), CEVA (CEA)
Evolution of electron distribution function (phase space density) with empirical diffusion coefficients derived from statistical wave models

Quasi-linear theory assumes that :

- the distribution function evolves slowly compared to the gyroperiod of the particles and the wave period.
- the fluctuation amplitude is small and that the spatial average of the fluctuations vanishes

Waves included in radiation belt modeling

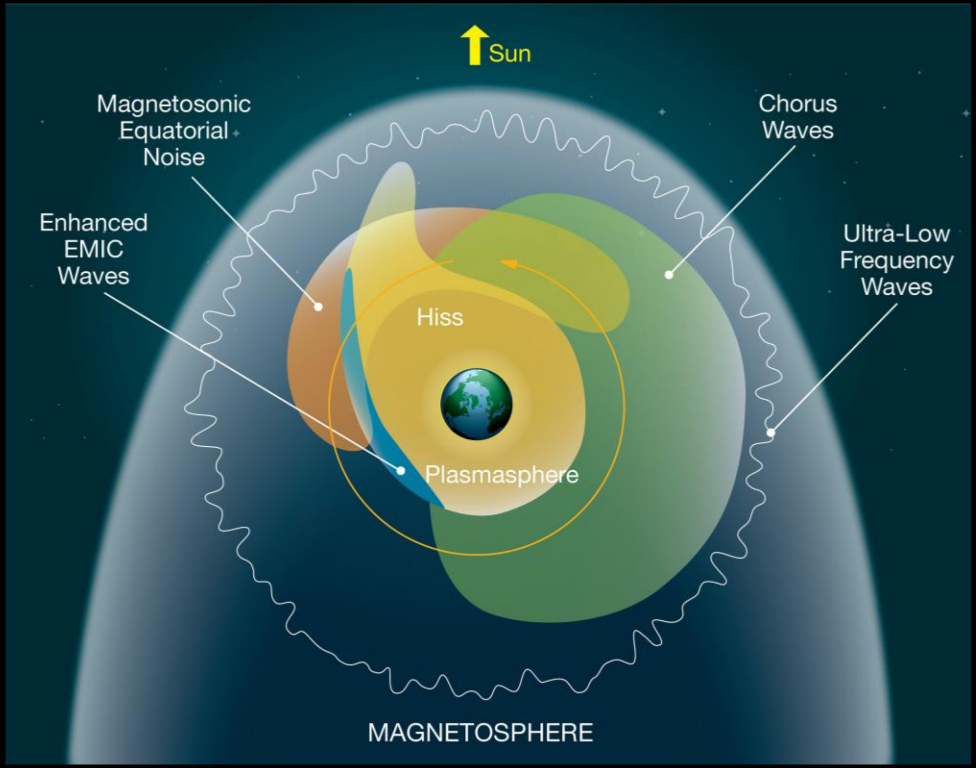

Locations of different wave types that may interact with radiation belt electrons as they drift around the Earth.
Credit: NASA

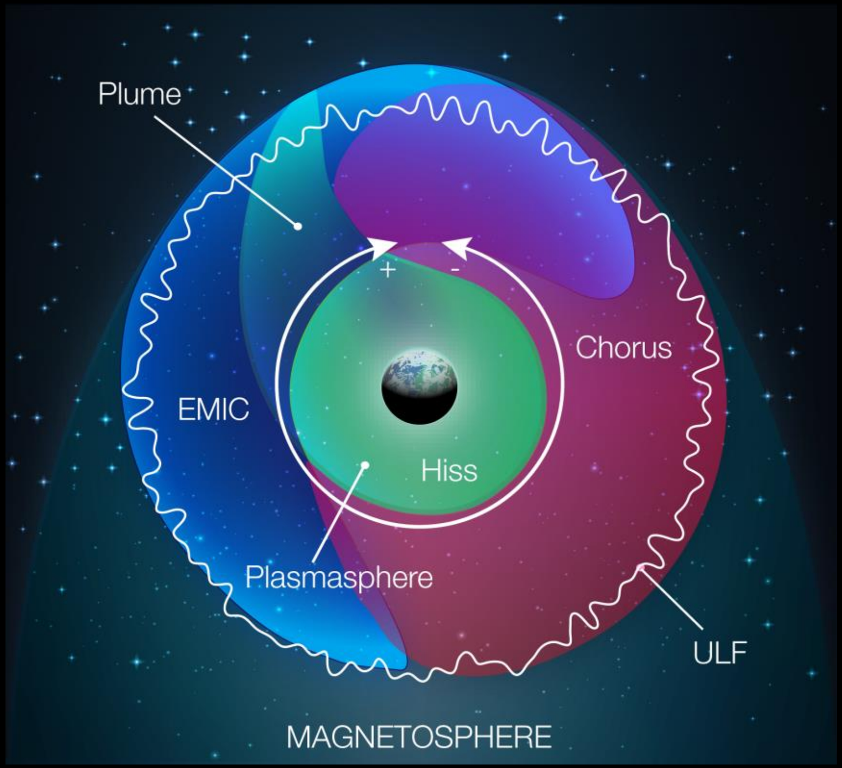

Statistical wave distributions based on satellite data. Usanova et al., in prep

Evolution of electron flux: VERB simulations

- VERB: versatile electron radiation belt code (Subbotin and Shprits, 2009)
- Solves the Fokker-Planck (diffusion) equation to look at the evolution of electron flux
- Uses statistical wave maps
- Allows to switch on and off different wave modes

The goal is to parameterize wave occurrence depending on solar wind parameters and geomagnetic activity indices

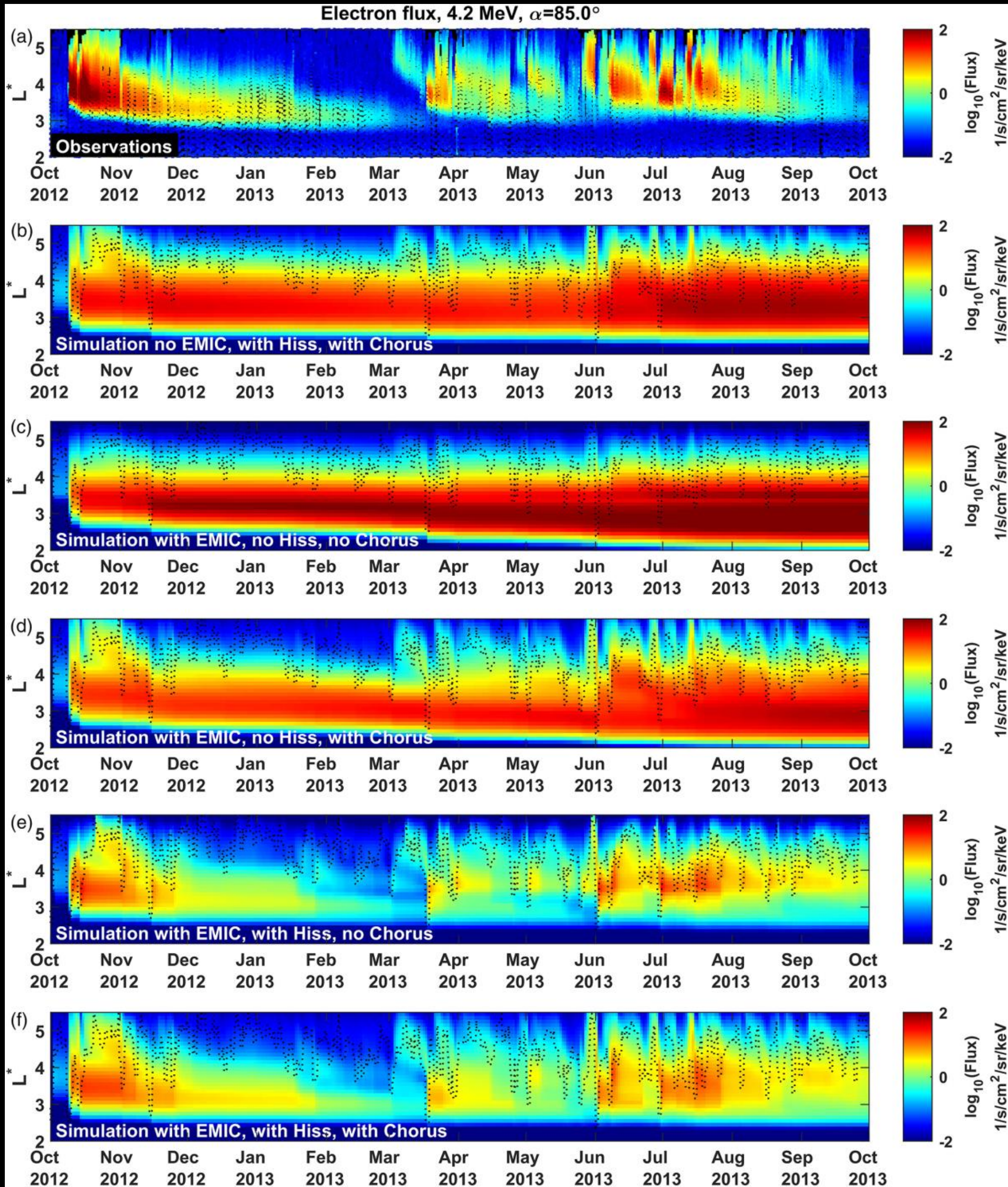

Drozdov, Usanova et al., 2020

Non-linear EMIC waves: rising tones

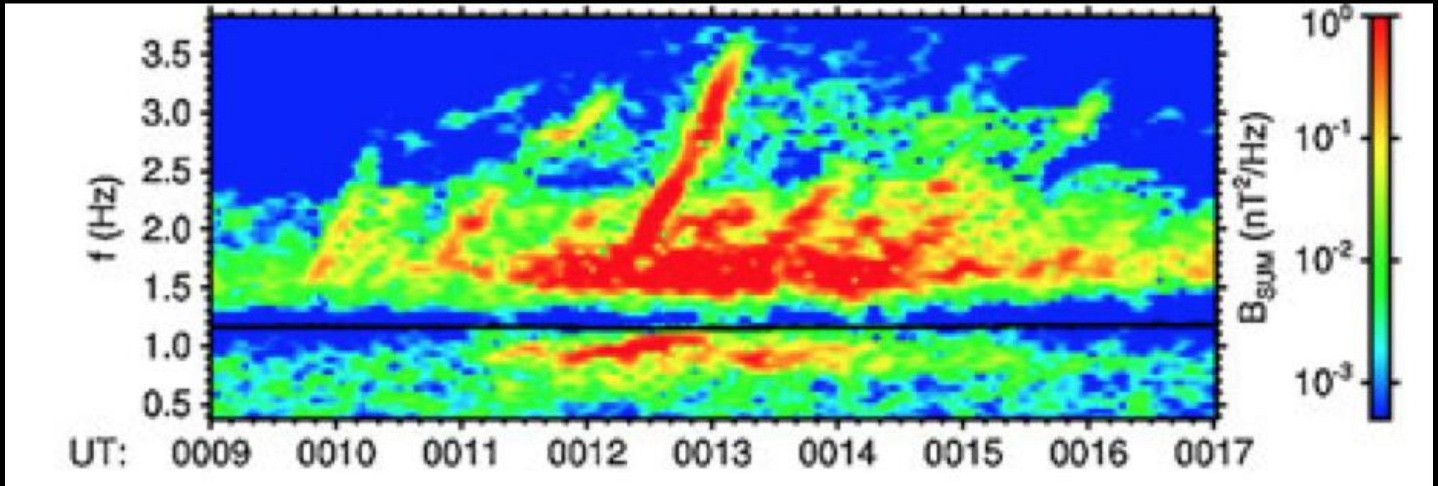

Cluster EMIC waves: Grison, 2013

Non-linear wave particle-interaction causes effective pitch angle scattering and can induce relativistic electron microbursts (Omura et al., 2008; Omura and Zhao, 2013).

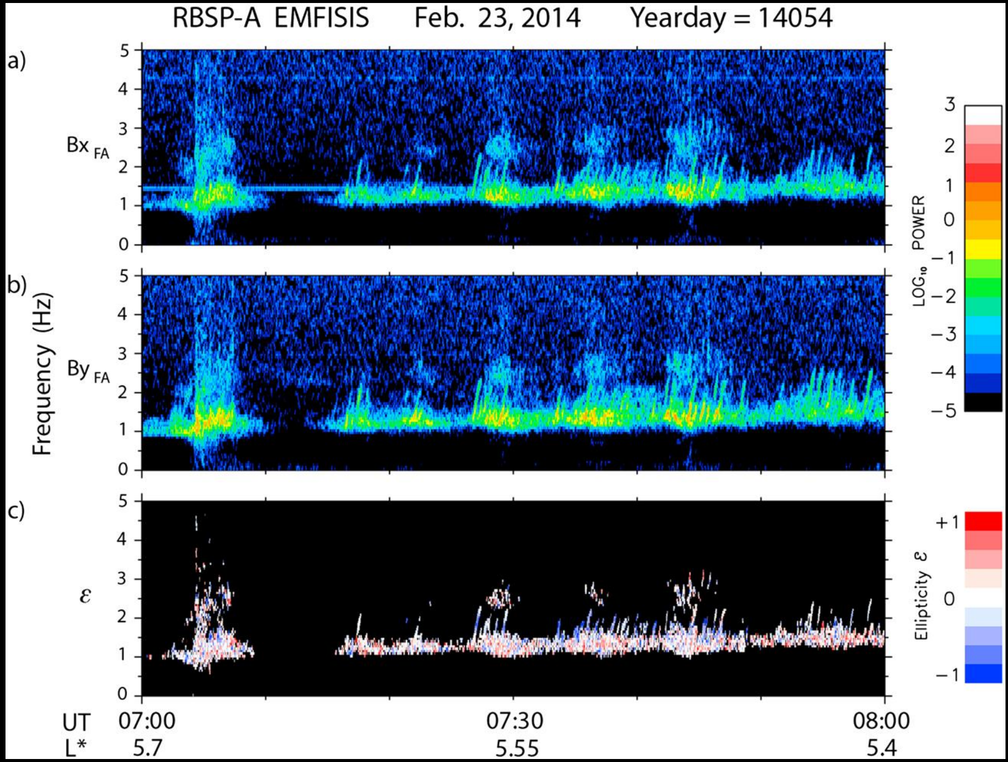

EMIC-triggered emissions appeared during the strongest compression

Engebretson et al., 2015

EMIC rising and falling tone emissions observed by THEMIS

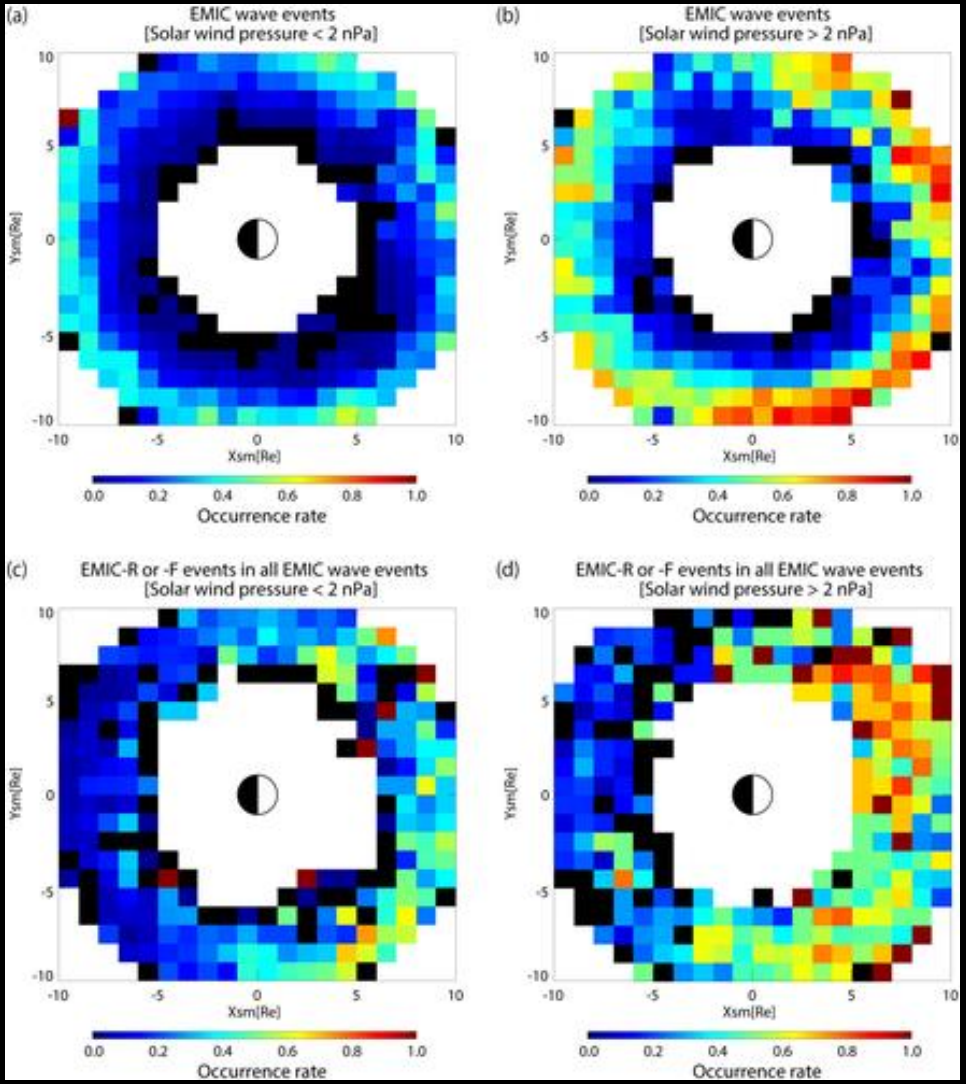

Nakamura et al., 2016

- More than 30% of EMIC waves contain rising or falling tones on the dayside magnetosphere
- The occurrence of rising or falling tones strongly depend on the solar wind pressure
- Large-amplitude waves have wide frequency variations and subpacket structures

Modulation of EMIC waves by ULF waves

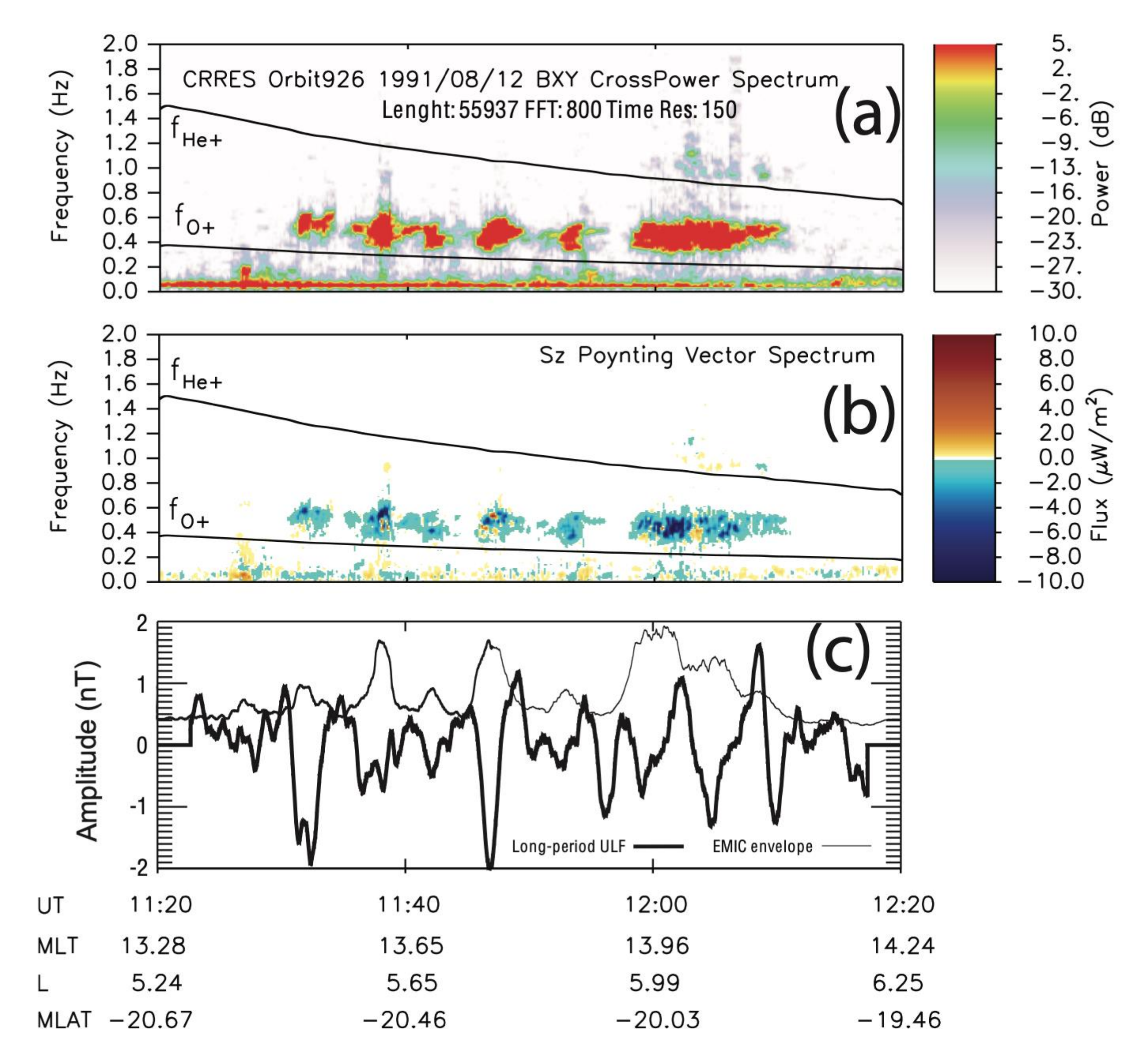

CRRES observations, Loto'aniu et al., 2009

Anti-phase modulation may be explained by a decreasing background magnetic field due to the negative cycle of the ULF wave decreasing EMIC wave instability threshold.

High frequency growth modulation by EMIC waves

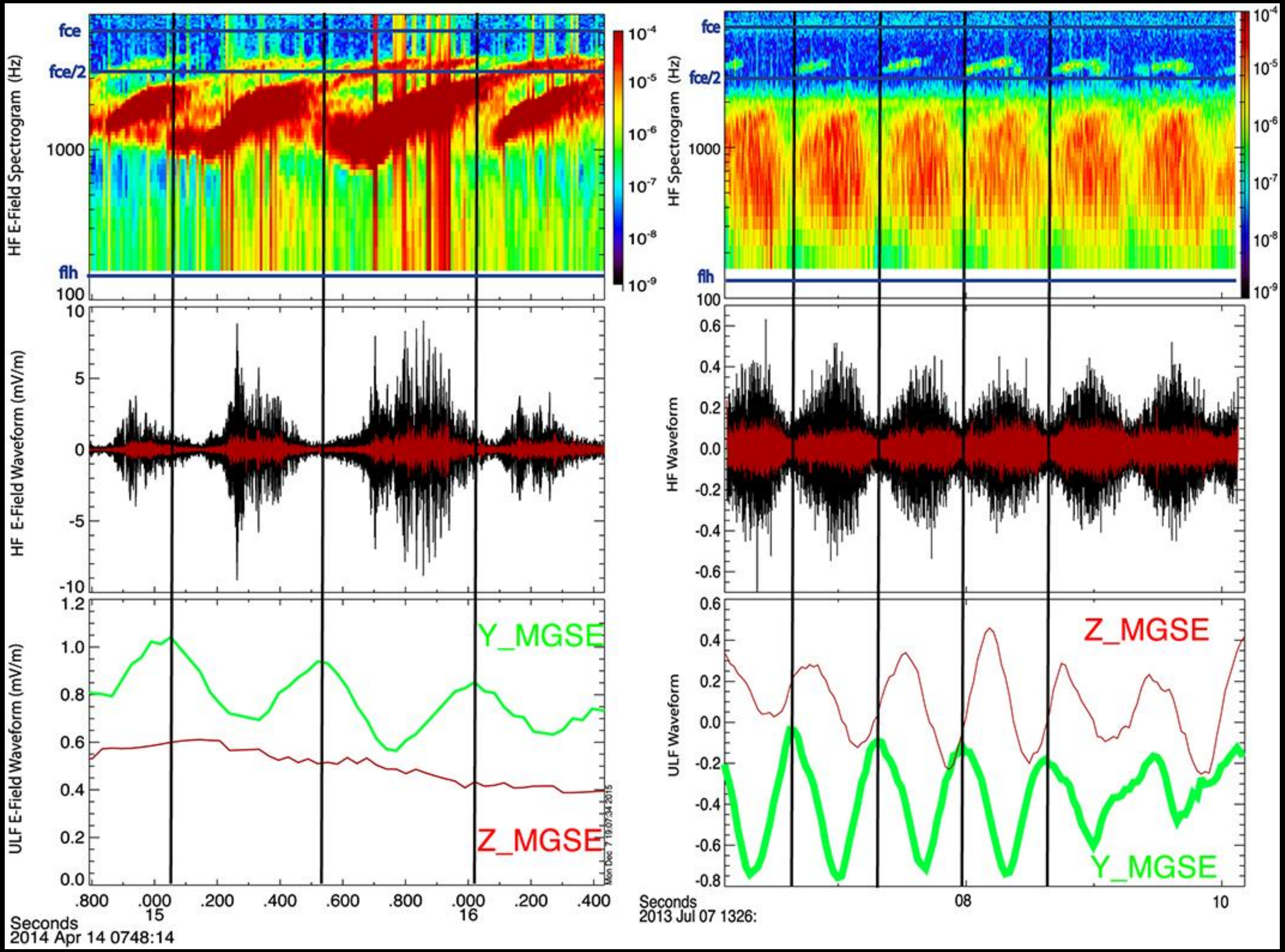

(left) 14 April 2014 07:48:14 - 07:48:17 UT harmonic
(right) 7 July 2013 13:26:06 - 13:26:10 UT: EMIC
(top) 100–8000 Hz wave electric field; (middle) parallel (red) and perpendicular (black) E-field components; (bottom) 0–5 Hz wave B-field in the *Z* (red) and *Y* (green) component in the MGSE

Colpitts et al., 2016; Usanova et al., 2018

Energetic particle precipitation into the atmosphere

Produces changes in atmospheric chemistry and may have potential effects on weather systems

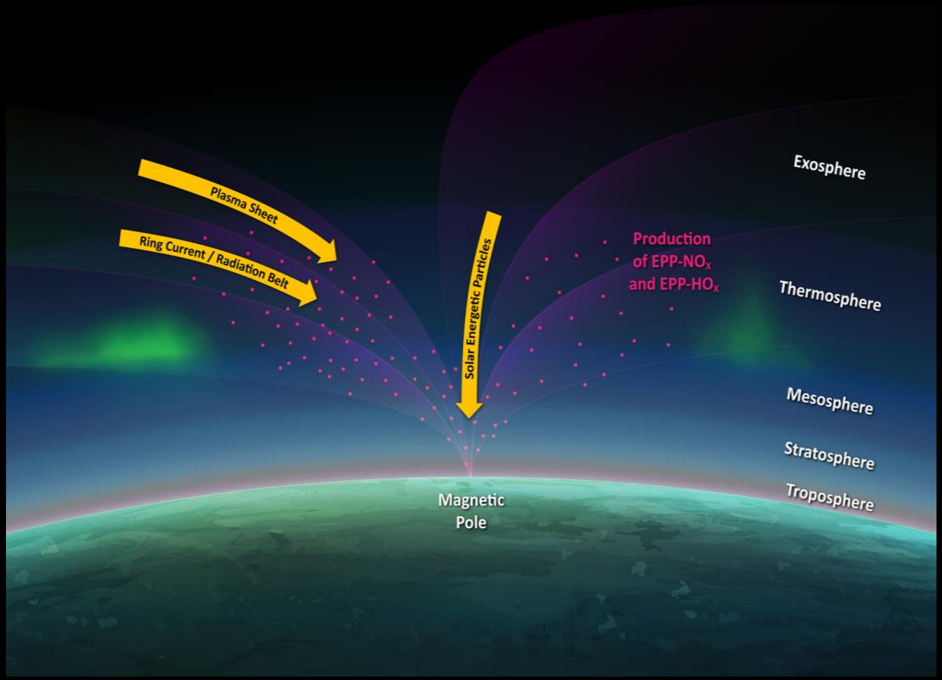

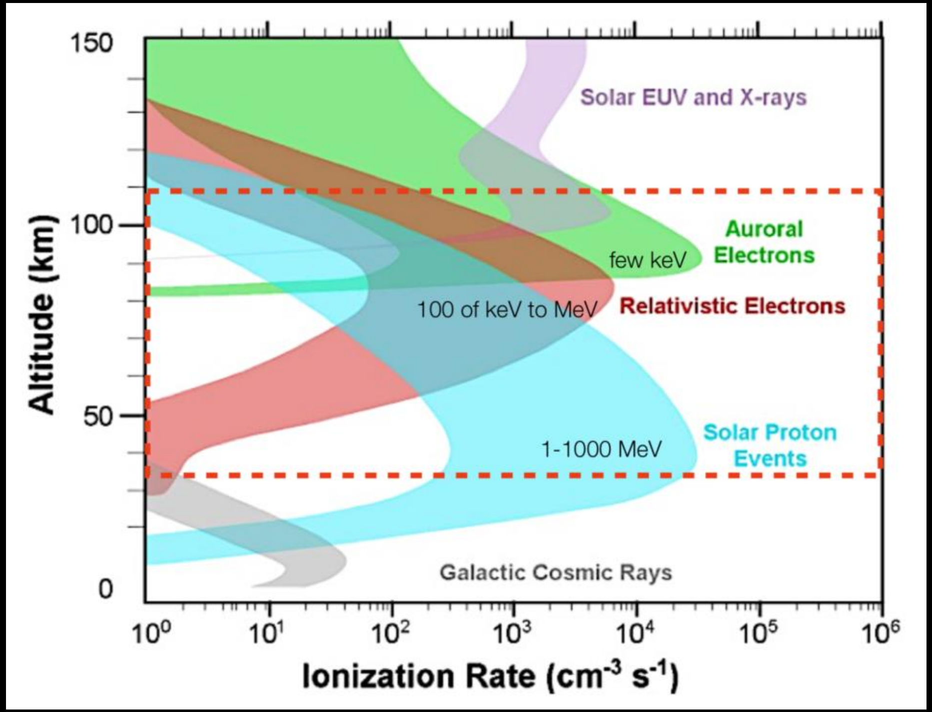

Baker, 2012

Linkage to polar climate

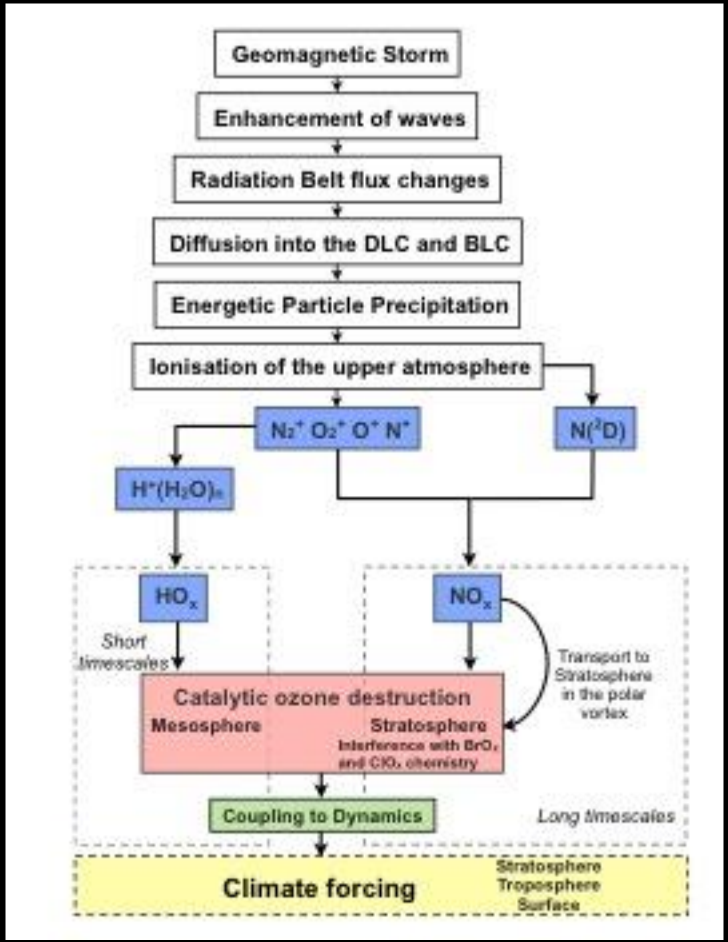

Clilverd et al., OUP, 2016

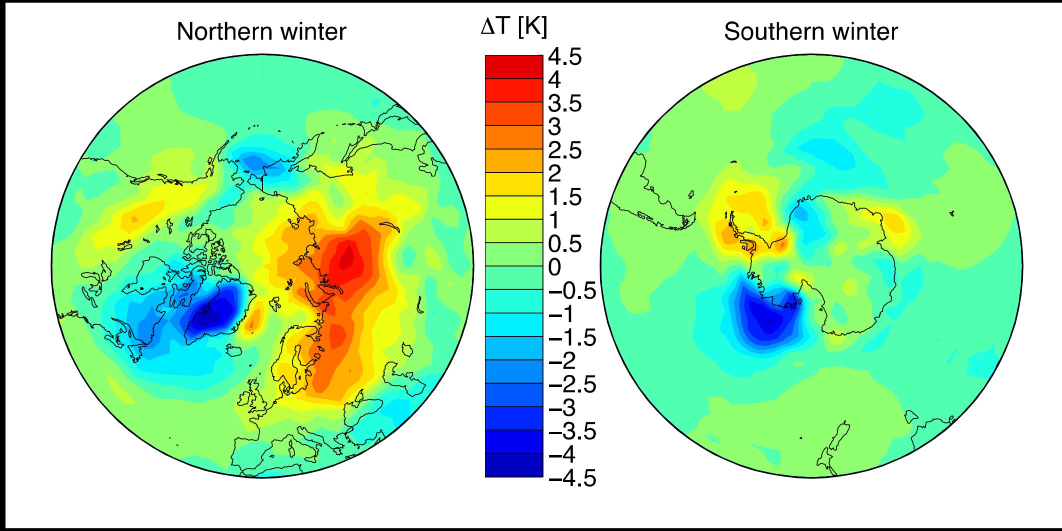

Electron precipitation contributes to the production of odd nitrogen NOx (N + NO + NO_2) through the dissociation of molecular nitrogen, and odd hydrogen HO_x (H + OH + HO_2) which in turn destroy O_3.
Changes in the radiative balance of the atmosphere can lead to ±5K variations in polar surface temperature (Seppala et al. 2009).

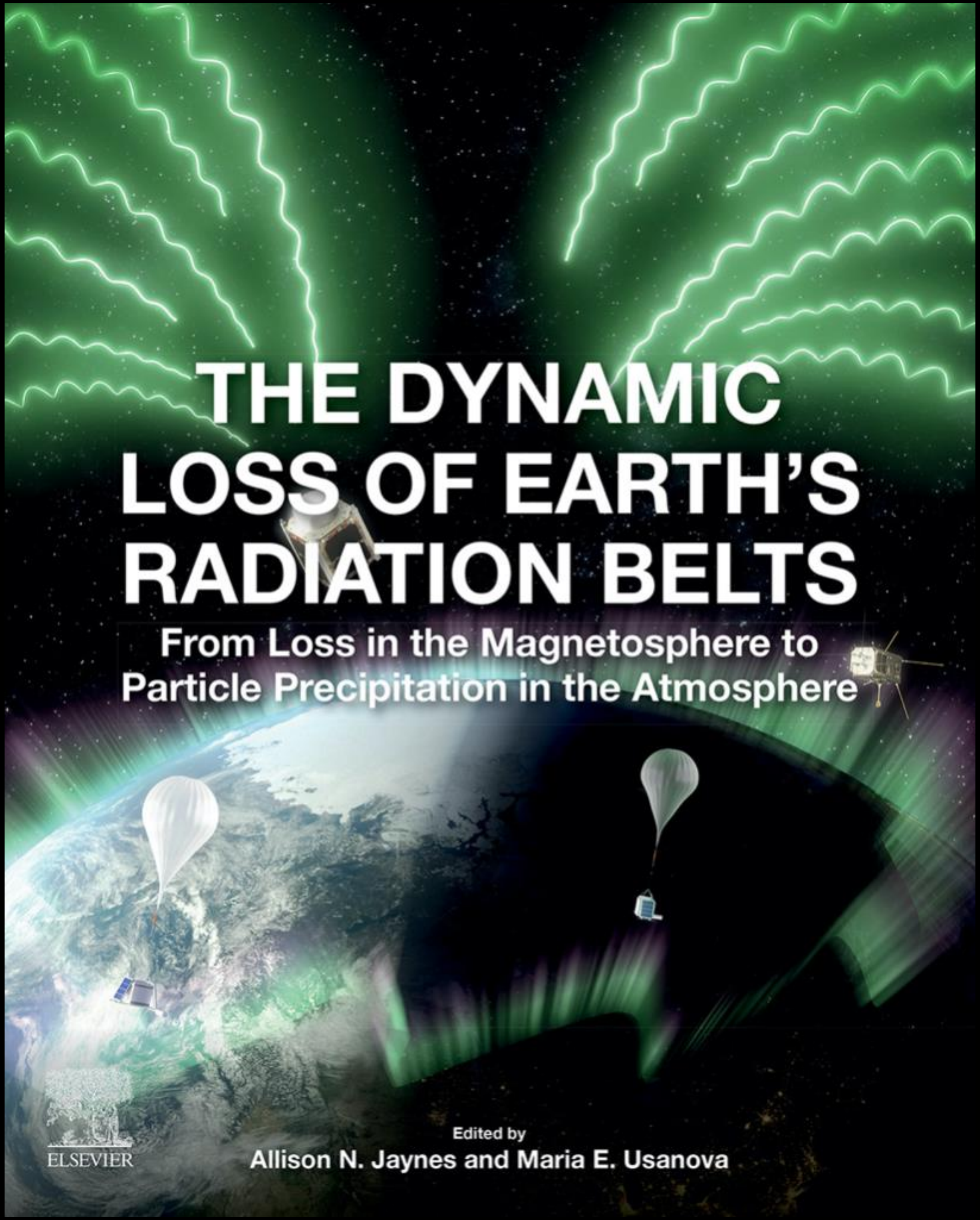

THE DYNAMIC LOSS OF EARTH'S RADIATION BELTS

From Loss in the Magnetosphere to Particle Precipitation in the Atmosphere

Edited by
Allison N. Jaynes and Maria E. Usanova

ELSEVIER

Magnetospheres of other magnetized planets (Jupiter, Saturn, Uranus, Neptune)

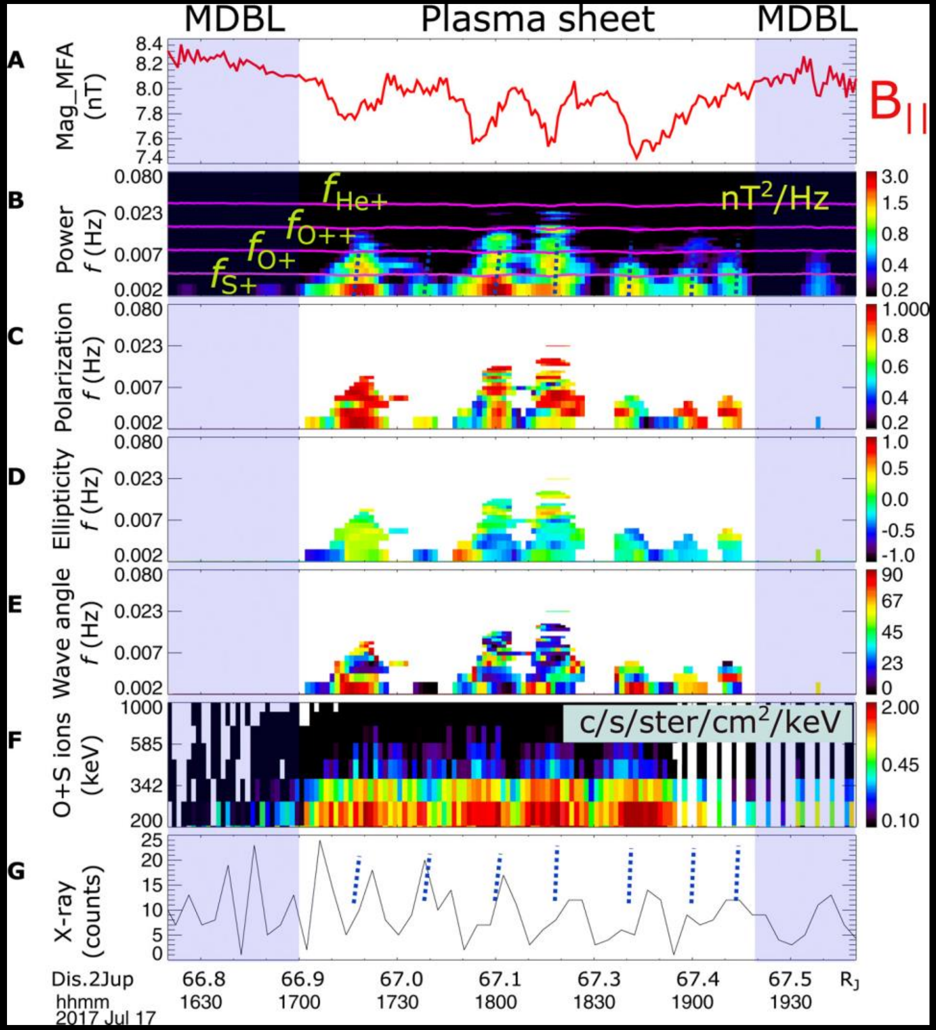

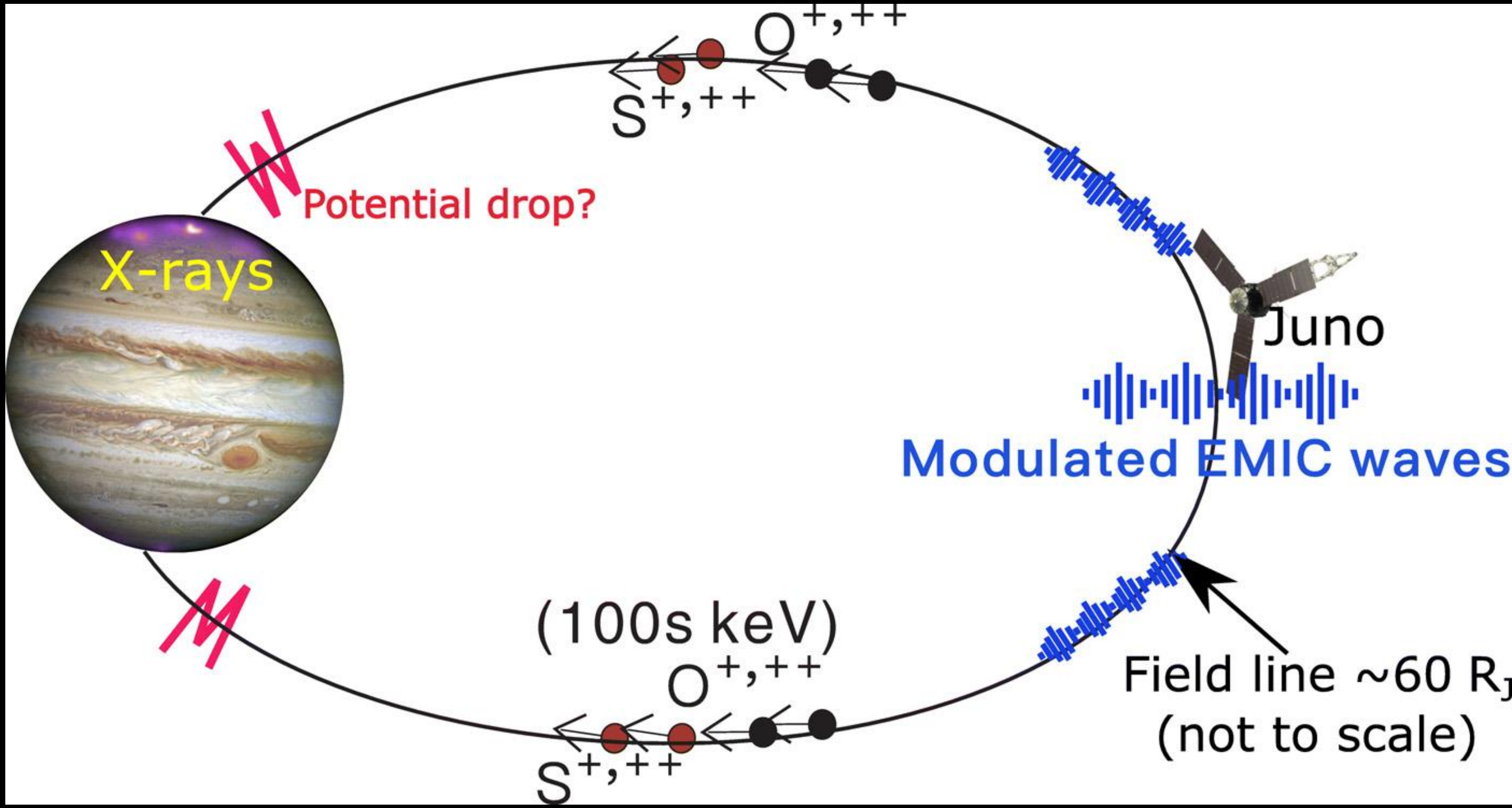

Jupiter's X-ray emissions as a result of EMIC-driven heavy ion precipitation
Yao et al., 2021

Summary: the role of EMIC waves in energy coupling

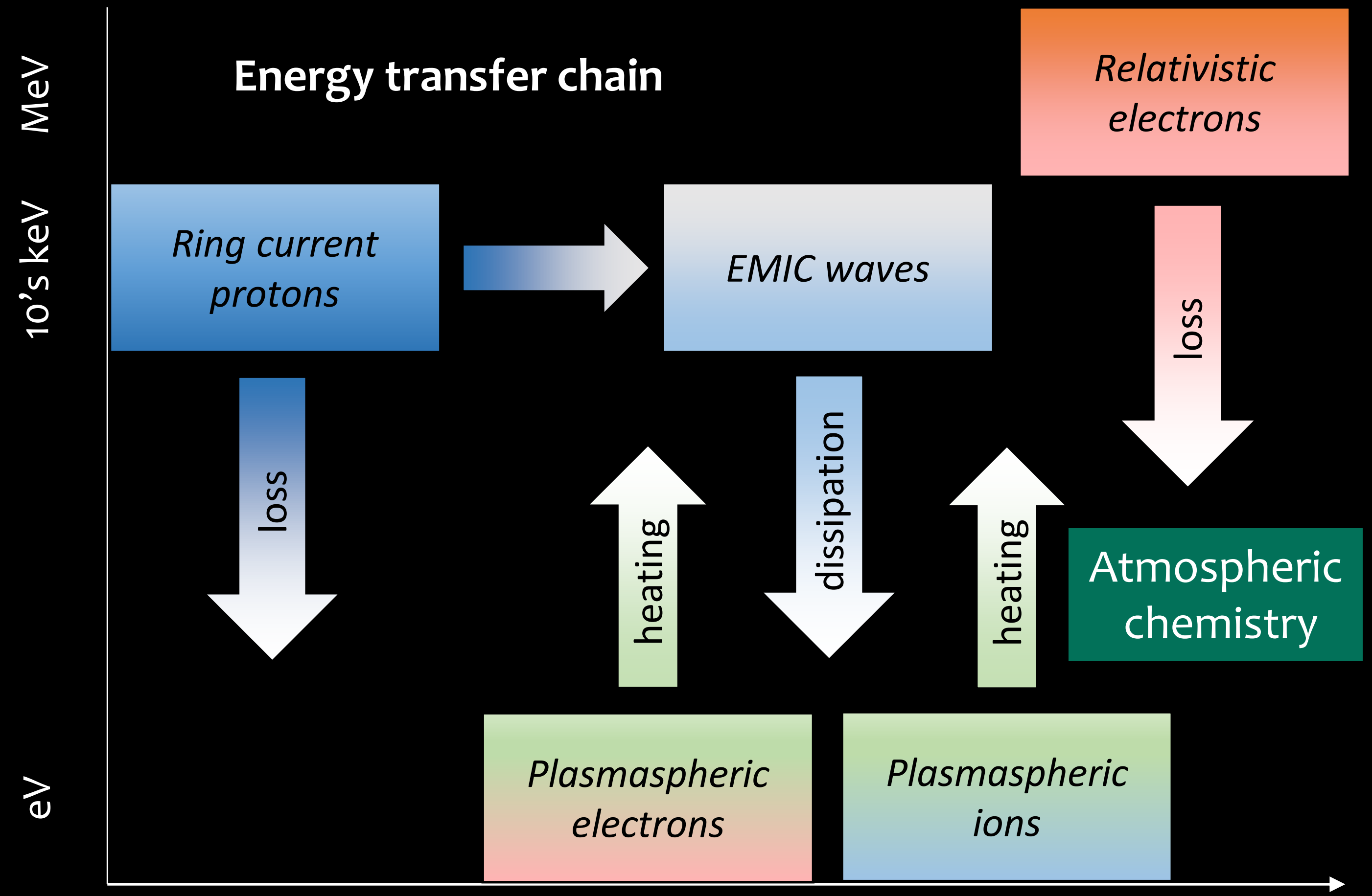

Usanova, 2021

Summary

- EMIC waves are an important element of magnetospheric environment
- They contribute to:
  - Loss of energetic particles, both ions and electrons
  - Heating of cold plasma
  - Cross-energy coupling between eV, keV and MeV populations
  - Potentially, climate forcing through energetic particle precipitation
- Observed in other planetary environments
- Comprehensive knowledge about EMIC-driven energy-exchange processes and their relative importance and distribution in space and time is needed to improve physics-based models
- Accurate parametrization as a function on solar wind and geomagnetic conditions is warranted
- Recent studies emphasized the role of nonlinear processes in EMIC wave-particle interactions and the potential to include them in global magnetospheric models which will be a next crucial step towards predictive modeling